

YARKOVSKY DRIFT DETECTIONS FOR 159 NEAR-EARTH ASTEROIDS

ADAM H. GREENBERG,¹ JEAN-LUC MARGOT,¹ ASHOK K. VERMA,¹ PATRICK A. TAYLOR,² AND SUSAN E. HODGE³

¹*University California, Los Angeles, CA*

²*Arecibo Observatory, Universities Space Research Association, Arecibo, PR*

³*Nationwide Children's Hospital, Columbus, OH*

ABSTRACT

The Yarkovsky effect is a thermal process acting upon the orbits of small celestial bodies, which can cause these orbits to slowly expand or contract with time. The effect is subtle – typical drift rates lie near 10^{-4} au/My for a ~ 1 km diameter object – and is thus generally difficult to measure. However, objects with long observation intervals, as well as objects with radar detections, serve as excellent candidates for the observation of this effect. We analyzed both optical and radar astrometry for all numbered Near-Earth Asteroids (NEAs), as well as several un-numbered NEAs, for the purpose of detecting and quantifying the Yarkovsky effect. We present 159 objects with measured drift rates. Our Yarkovsky sample is the largest published set of such detections, and presents an opportunity to examine the physical properties of these NEAs and the Yarkovsky effect in a statistical manner. In particular, we confirm the Yarkovsky effect's theoretical size dependence of $1/D$, where D is diameter. We also examine the efficiency with which this effect acts on our sample objects and find typical efficiencies of around 12%. We interpret this efficiency with respect to the typical spin and thermal properties of objects in our sample. We report the ratio of negative to positive drift rates in our sample as $N_R/N_P = 2.9 \pm 0.7$ and interpret this ratio in terms of retrograde/prograde rotators and main belt escape routes. The observed ratio has a probability of 1 in 46 million of occurring by chance, which confirms the presence of a non-gravitational influence. We examine how the presence of radar data affects the strength and precision of our detections. We find that, on average, the precision of radar+optical detections improves by a factor of approximately 1.6 for each additional apparition with ranging data compared to that of optical-only solutions.

Keywords: asteroids, Yarkovsky, orbit-determination, radar-astrometry

1. INTRODUCTION

The Yarkovsky effect is a small force that results from the anisotropic thermal emission of small celestial bodies. Over the past decade, there has been increasing awareness that the Yarkovsky effect plays an important role in the evolution of asteroid orbits and the delivery of meteorites to Earth (Bottke et al. 2006). Several authors have published Yarkovsky effect detections for dozens of asteroids: Chesley et al. (2008, 12 detections), Nugent et al. (2012, 54 detections), Farnocchia et al. (2013, 47 detections, of which 21 are deemed reliable).

Here, we provide the largest collection of Yarkovsky detections to date and introduce several improvements to previous studies. Nugent et al. (2012) and Farnocchia et al. (2013) relied on the debiasing of star catalogs proposed by Chesley et al. (2010). Our current model uses the more up-to-date and accurate debiasing algorithm of Farnocchia et al. (2015). Previous works have traditionally relied on a signal-to-noise (S/N) metric and the quantity and quality of the observational data to distinguish between detections and non-detections (Chesley et al. 2008; Farnocchia et al. 2013), or by augmenting these criteria with an explicit sensitivity metric (Nugent et al. 2012). Here, we further refine the detection criterion with a precise formulation based on an analysis of variance (Greenberg et al. 2017). Some of the previous formulations (e.g., Nugent et al. 2012) included a finite increment in semi-major axis at each time step irrespective of the asteroid’s distance from the Sun. Here, we use a $1/r^2$ dependence of the solar flux. The Nugent et al. (2012) results were based on astrometry obtained as of January 31, 2012. The current work benefits from more than 5 years of additional astrometry, including more than 100 additional ranging observations with the Arecibo and Goldstone radars. Finally, the numbers of known NEAs and numbered NEAs have both nearly doubled since the Nugent et al. (2012) study. The number of detections is now sufficiently large that ensemble properties can be refined, such as the ratio of retrograde to prograde rotators, and the physical theory can be tested, such as the dependence of the Yarkovsky drift magnitude as a function of asteroid size.

2. DATA PREPARATION

Optical astrometry was automatically downloaded from the Minor Planet Center (MPC) on Mar 8, 2017 (Minor Planet Center 2017). Astrometry taken from non-stationary (generally, space-based) observatories was discarded. Radar astrometry was downloaded from the JPL Radar Astrometry Database (JPL Solar System Dynamics 2017a) and was discarded from MPC records to avoid duplication. In a few instances, previ-

ously unpublished radar data obtained by the authors were also used.

2.1. Weighting and debiasing

Optical astrometry was weighted following the methods described by Farnocchia et al. (2015). To summarize, this method involved weighting measurements based on the observatory, type of measurement, star catalog, and date. We also used the “batched weighting” scheme described by Farnocchia et al. (2015), wherein measurements taken from the same observatory on the same night were given a smaller weight. Star catalog debiasing was also performed according to the approach of Farnocchia et al. (2015).

Radar astrometry was weighted according to observer-reported uncertainties.

2.2. Outlier rejection

Outlier rejection was performed via an iterative fit-drop-add scheme. All available data were used during the initial gravity-only orbital fit. Then all optical measurements with weighted residuals beyond a fiducial threshold were rejected. Radar data were excluded from outlier rejection. This threshold was defined as

$$\frac{(O_{i,RA} - C_{i,RA})^2}{\sigma_{i,RA}^2} + \frac{(O_{i,DEC} - C_{i,DEC})^2}{\sigma_{i,DEC}^2} < 8, \quad (1)$$

where O and C stand for observed and computed values, respectively, RA and DEC stand for right ascension and declination, respectively, σ represent observational uncertainty, and the index i represents the i^{th} observation.

As the fit iterated, previously discarded measurements were re-evaluated with respect to this threshold, and included in subsequent iterations, as appropriate. Outlier rejection was disabled after three fit-drop-add iterations gave identical results.

Initially, outlier rejection was performed with a gravity-only model. After the Yarkovsky component of the dynamical model was estimated, outlier rejection was performed once more with the additional Yarkovsky component included (Section 4).

3. ORBIT DETERMINATION

Orbit determination was performed using our Integration and Determination of Orbits System (IDOS, see Greenberg et al. (2017)). At its core, this software utilizes the Mission analysis, Operations, and Navigation Toolkit Environment (MONTE), a set of tools developed by the Jet Propulsion Laboratory (JPL) for a variety of space-related science and aeronautical goals (Evans et al. 2016). The MONTE orbital integrator can account for gravitational perturbations from any set of

masses – for the analyses performed in this paper, we considered the eight known planets and 24 of the most massive minor planets (Folkner et al. 2014) as gravitational perturbers. During close Earth approaches, the integrator considers a detailed model of the planetary gravitational field. MONTE also accounts for general relativistic effects during orbital integration. Further details concerning the internal operations of IDOS were described by Greenberg et al. (2017).

In gravity-only solutions, we estimated the six parameters (three position and three velocity components) of the state vector simultaneously. In Yarkovsky solutions, we estimated an additional parameter describing the strength of the Yarkovsky drift. We assigned one-standard-deviation uncertainties (σ) to our Yarkovsky estimates such that a 1- σ change to the drift rate results in an increase of one in the sum of squares of weighted residuals, similar to the approach of Nugent et al. (2012). This approach yields values that match the formal uncertainties derived from a covariance matrix, which was the approach of Farnocchia et al. (2013).

4. YARKOVSKY FORCE MODEL

We utilized the Yarkovsky force model described by Greenberg et al. (2017), where the magnitude and direction of the thermal acceleration, \ddot{r} , is calculated and applied at every integration time step of the dynamical model. The acceleration is calculated as

$$\ddot{\vec{r}} = \zeta \frac{3}{8\pi} \frac{1}{D\rho} \frac{L_{\odot}}{c} \frac{X_{\hat{p}}(\phi)\vec{r}(t)}{\|\vec{r}(t)\|^3}, \quad (2)$$

where $\vec{r}(t)$ is the heliocentric radial vector for the object at time t , \hat{p} is the unit spin-axis vector, ϕ is the phase lag, L_{\odot} is the luminosity of the Sun, c is the speed of light, and $X_{\hat{p}}(\phi)$ is the rotation matrix about p . D and ρ are the diameter and density of the object, respectively, while ζ is an efficiency factor. The phase lag ϕ describes the longitude on the surface from which photons are re-emitted, relative to the sub-Solar longitude. In Equation 2, we assume a perfect absorber, i.e., a Bond albedo of zero.

For the objects analyzed in this work, specific values for ϕ and \hat{p} were not known. Therefore, these values were fixed at 90° and anti-parallel to the orbit normal vector, respectively, which maximizes the magnitude of the orbital perturbation. As we discuss in the next paragraph, these assumptions do not affect the estimated value of the semi-major axis drift.

With knowledge of the orbit semi-major axis, a , and eccentricity, e , the orbit-averaged drift in semi-major axis, $\langle da/dt \rangle$, can be determined from this acceleration

model with

$$\langle da/dt \rangle = \pm \xi \frac{3}{4\pi} \frac{1}{\sqrt{a}} \frac{1}{1-e^2} \frac{L_{\odot}}{c\sqrt{GM_{\odot}}} \frac{1}{D\rho}, \quad (3)$$

which is equivalent to Greenberg et al. (2017)'s equation (8) and corrects Nugent et al. (2012)'s equation (1). Here, ξ is the Yarkovsky efficiency, and depends on ζ , spin pole obliquity γ (i.e., the angle between the spin pole vector \hat{p} and the orbit normal vector), and phase lag ϕ . We always take the Yarkovsky efficiency to be positive. Any incorrect assumption about Bond albedo, diameter, obliquity, and phase lag are absorbed in this efficiency factor such that the $\langle da/dt \rangle$ value, which is dictated by the astrometry, is not affected by these assumptions (Section 14.3).

With numerical values, we find

$$\langle da/dt \rangle = \pm 1.45 \left(\frac{\xi}{0.01} \right) \left(\frac{1 \text{ au}}{a} \right)^{\frac{1}{2}} \left(\frac{1}{1-e^2} \right) \times \left(\frac{1 \text{ km}}{D} \right) \left(\frac{1000 \text{ kg m}^{-3}}{\rho} \right) \times \frac{10^{-4} \text{ au}}{\text{My}}. \quad (4)$$

5. CANDIDATE SELECTION

5.1. Initial selection

We considered three sets of Yarkovsky detection candidates. Two sets of candidates, the **Nugent12** set and the **Farnocchia13** set, represent Yarkovsky detections reported by Nugent et al. (2012) and Farnocchia et al. (2013), respectively. For these objects, we performed our analysis in two ways – first, by using the same observational data as that used by the authors, and second, by using all currently available data (Section 5.2). The **Nugent12** set features 54 objects, while the **Farnocchia13** set contains 47 objects.

The third data set, **UCLA17**, contains objects that had not previously been considered by the other two works but that we determined to be Yarkovsky detection candidates. For the most part, these objects had either not yet been discovered, or had small observation intervals prior to 2012 or early 2013. We identified the new candidates as follows. First, we downloaded the list of 15,595 known NEAs from the MPC on March 7, 2017. Second, for each one of the 2,348 numbered NEAs, we computed the Yarkovsky sensitivity metric (s_Y) described by Nugent et al. (2012). This root-mean-square quantity provides an excellent assessment of the relative sensitivity of selected data sets to drifts in semimajor axis. We used the threshold determined by Nugent et al. (2012) of $s_Y > 2$. Only 376 NEAs met this condition. Third, we computed preliminary estimates of $\langle da/dt \rangle$ and associated uncertainties for these 376 NEAs. We defined a signal-to-noise (S/N) metric as the ratio of the best-fit

$\langle da/dt \rangle$ to its one-standard-deviation uncertainty. We selected the 200 NEAs that have both $s_Y > 2$ and $S/N > 1$. Of these, 59 had been previously considered by Nugent et al. (2012) or Farnocchia et al. (2013).

Nugent et al. (2012) rejected Yarkovsky detections for which there were fewer than 100 astrometric measurements, or for which the observation interval was less than 15 years. However, we reviewed the detections that were discarded due to these criteria in 2012 and found that 90% of them were reliable, i.e., their $\langle da/dt \rangle$ values are consistent with values presented in this work, even after the addition of post-2012 data. In this work, we flag objects that Nugent et al. (2012) would have discarded because of data span or quantity, but we do not discard the detections.

Among the three sets of objects (Nugent12, Farnocchia13, and UCLA17), there are 231 distinct Yarkovsky candidates.

5.2. Selection refinement

After candidate selection, we performed a six-parameter fit to the astrometry using a gravity-only model, followed by a seven-parameter fit which included a Yarkovsky force model. We then performed an *analysis of variance* (Mandel 1964) to determine whether the data warrants the use of the Yarkovsky model.

Specifically, we calculated the test-statistic

$$F = \frac{\kappa_\delta}{\kappa_Y} \quad (5)$$

where

$$\kappa_\delta = \frac{\sum_{i=0}^N \left(\frac{O_i - C_{0,i}}{\sigma_i}\right)^2 - \sum_{i=0}^N \left(\frac{O_i - C_{Y,i}}{\sigma_i}\right)^2}{m_Y - m_0} \quad (6)$$

and

$$\kappa_Y = \frac{\sum_{i=0}^N \left(\frac{O_i - C_{Y,i}}{\sigma_i}\right)^2}{N - m_Y}. \quad (7)$$

Here, $C_{0,i}$ is the i^{th} computed value assuming gravity only, $C_{Y,i}$ is the i^{th} computed value assuming our best-fit Yarkovsky model, O_i is the i^{th} observation and σ_i is the measurement uncertainty for that observation, N is the number of observations, and m_Y , m_0 are the number of free parameters in the Yarkovsky model ($m_Y = 7$) and gravity-only model ($m_0 = 6$), respectively.

We then calculated the value

$$p = \int_{x=F}^{x=\infty} f(m_Y - m_0, N - m_Y, x) dx, \quad (8)$$

where $f(m_Y - m_0, N - m_Y, x)$ is the F-distribution probability density function with $m_Y - m_0$ and $N - m_Y$ degrees of freedom. The p -value serves as a metric for

testing the null hypothesis — namely, that the additional degree of freedom introduced by the Yarkovsky force model is superfluous.

Our initial selection refinement step consisted of discarding those objects for which $p > 0.05$, which approximately corresponds to a 2-standard-deviation detection threshold. This step rejected 60 objects, leaving 171 objects for further consideration.

We also followed the procedure of Nugent et al. (2012), and determined those objects for which there were fewer than 10 measurements in the first 10 years of observations. This check is necessary because isolated, erroneous astrometry can result in spurious detections. For these objects, we re-fit the Yarkovsky model with the sparse observations removed, and rejected any objects for which the resulting $\langle da/dt \rangle$ value changed significantly from that of the nominal fit. This step rejected 12 objects, leaving 159 objects remaining. These 159 asteroids make up our final set of Yarkovsky detections (Table 1).

Finally, because pre-CCD astrometry can lead to spurious detections (Section 13.7) even with proper weights, we re-analyzed 27 Yarkovsky candidates for which pre-1965 astrometry exists. Specifically, we discarded the pre-1965 astrometry, fit for $\langle da/dt \rangle$ values with the shortened observation intervals, and recomputed p -values. Objects that no longer met the $p \leq 0.05$ criterion were flagged. About a dozen objects are in this category and their Yarkovsky rates require additional verification.

6. COMPARISON WITH PREVIOUS WORKS

Many of the objects considered for this work had been previously reported as Yarkovsky detections (Section 5). It is useful to compare our Yarkovsky determinations to these previous works, for two reasons. First, because our results were determined independently of the previous works, a comparison serves as a check on both sets of results. Second, new astrometry has been reported for many of these objects. Therefore, we can study how the results and uncertainties changed in light of new data.

We performed two comparisons with the previous works. In each case, we compared both our absolute Yarkovsky measurements and their associated uncertainties to those of the original works. We first created data sets that roughly matched the observational intervals reported by previous authors, to the nearest calendar year. In doing so, we expect there to be good agreement between our Yarkovsky detections and those of the original works. We do anticipate slight differences introduced by our use of improved debiasing and weighting algorithms (Section 2.1) and by our use of observation

sets that are not identical to those used in the original works (e.g., observations at beginning or end of intervals matched to the nearest calendar year, precovery observations, or observations that were re-measured). For our second comparison, we included all available data for all objects. In this case, we expect an overall lower level of agreement because of our use of additional astrometry, which sometimes represent a significant fraction of the available astrometry.

Because we are interested in whether our results match those previously published, it is useful to quantify what we mean by a “match”. We used a metric inspired by mean-comparison tests. Namely, for each object i in the dataset, we calculated

$$z_i = \frac{|Y_{t,i} - Y_{p,i}|}{\sqrt{\sigma_{t,i}^2 + \sigma_{p,i}^2}}, \quad (9)$$

where $Y_{t,i}, Y_{p,i}$ are this work’s estimated drift rate for object i and the previous work’s estimated drift rate for object i , respectively, and $\sigma_{t,i}, \sigma_{p,i}$ are this work’s uncertainty for object i and the previous work’s uncertainty for object i , respectively. The quantity z therefore repre-

sents a significance score. By choosing a threshold value for z , we can signal our confidence that our measurement is consistent with that of the original work. We chose a significance threshold of 2.0, i.e., detection i was considered a match if

$$z_i < 2.0. \quad (10)$$

In other words, we concluded that the two measurements matched if we could not reject the hypothesis that the two measurements were drawn from the same distribution at the 95% confidence level.

7. YARKOVSKY DRIFT RATES

We measured semi-major axis drift rates and calculated Yarkovsky efficiency values for 159 NEAs, shown in Table 1 and ordered by object number. We present drift rates derived from optical measurements, as well as optical plus radar astrometry. An online, machine-readable file containing the data in this table can be found at <http://escholarship.org/uc/item/0pj991hd>.

Table 1. Yarkovsky drift measurements for 159 Near-Earth Asteroids. The semi-major axis, a , is in au. e is orbital eccentricity. Asteroid diameter D is in km. Diameters inferred from H-magnitude via Equation 14 are flagged with a *. N_o, N_r are the number of optical measurements and radar measurements, respectively. $\langle da/dt \rangle, \sigma$, the semi-major axis drift and associated uncertainty, are in au/My. For objects with radar astrometry ($N_r > 0$), we also report $\langle da/dt \rangle_r$ and σ_r , which incorporate those radar measurements. p and p_r are the p-values used in distinguishing between a gravity-only dynamical model and a Yarkovsky dynamical model using optical data only and optical plus radar data, respectively. s_Y is the Yarkovsky sensitivity parameter of Nugent et al. (2012). ξ indicates the Yarkovsky efficiency, which was computed with a bulk density that was inferred from the spectral type, if available (Section 10). Yarkovsky detections determined to be weaker because of the time span or quantity of astrometry (Section 5.1) are flagged with \dagger , whereas objects with anomalously high ξ values ($\xi > 0.5$) are flagged with \S . Objects that yield a drift rate detection with pre-1965 data but not without it (Section 5.2) are flagged with C .

Name	a	e	D	N_o	N_r	$\langle da/dt \rangle$	σ	p	$\langle da/dt \rangle_r$	σ_r	p_r	s_Y	ξ	Arc
(433) Eros ^C	1.46	0.22	16.84	7951	2	-0.58	0.2	1e-15	-0.58	0.2	1e-15	67.4	0.21	1900 – 2017
(719) Albert ^C	2.64	0.55	*2.82	1144	0	-5.73	5.1	5e-03	–	–	–	4.6	0.34	1911 – 2017
(1036) Ganymed ^{\S}	2.66	0.53	37.67	5087	1	-5.02	1.3	1e-16	-5.02	1.3	1e-16	7.0	4.12	1924 – 2017
(1566) Icarus	1.08	0.83	1.00	1221	23	-4.61	0.5	1e-16	-4.45	0.5	1e-16	36.8	0.02	1950 – 2015
(1685) Toro	1.37	0.44	3.40	2290	9	-1.45	0.4	3e-14	-1.55	0.4	1e-16	34.8	0.09	1948 – 2016
(1862) Apollo ^C	1.47	0.56	1.50	1548	17	-0.26	0.9	6e-01	-1.78	0.2	1e-16	30.7	0.04	1930 – 2017
(1864) Daedalus ^{\S}	1.46	0.61	3.70	1713	1	-9.28	6.2	3e-03	-11.27	6.0	3e-04	3.1	0.59	1970 – 2017
(1915) Quetzalcoatl ^{\dagger C}	2.54	0.57	0.50	52	1	-42.38	23.0	3e-02	-45.19	22.7	2e-02	4.0	0.41	1952 – 2005
(2059) Baboquivari ^{\S C}	2.65	0.53	*2.24	416	0	16.14	8.5	1e-03	–	–	–	4.9	0.72	1963 – 2016
(2061) Anza ^{\S C}	2.27	0.54	2.60	345	0	13.23	7.5	3e-03	–	–	–	5.2	0.63	1960 – 2016
(2062) Aten	0.97	0.18	1.10	905	7	-6.06	0.9	1e-16	-5.32	0.7	1e-16	24.9	0.10	1955 – 2017
(2063) Bacchus	1.08	0.35	*1.23	666	12	-6.96	2.1	2e-09	-6.22	1.9	1e-08	17.3	0.13	1977 – 2016
(2100) Ra-Shalom	0.83	0.44	2.30	1477	6	-3.71	1.0	1e-12	-2.25	0.8	1e-08	18.6	0.05	1975 – 2017

Table 1 continued

Table 1 (continued)

Name	a	e	D	N_o	N_r	$\langle da/dt \rangle$	σ	p	$\langle da/dt \rangle_r$	σ_r	p_r	s_Y	ξ	Arc
(2101) Adonis	1.87	0.76	0.60	116	5	-30.27	14.4	6e-03	-20.08	13.0	4e-02	4.6	0.12	1935 – 2013
(2102) Tantalus	1.29	0.30	1.65	671	0	-2.14	2.1	3e-02	–	–	–	12.1	0.06	1975 – 2017
(2340) Hathor	0.84	0.45	0.30	421	7	-16.92	0.8	1e-16	-17.30	0.7	1e-16	28.4	0.07	1976 – 2015
(3200) Phaethon	1.27	0.89	5.10	3693	1	-8.83	3.5	1e-07	-7.80	3.4	1e-06	3.4	0.15	1983 – 2017
(3361) Orpheus	1.21	0.32	0.30	647	0	6.28	1.6	1e-11	–	–	–	18.0	0.03	1982 – 2014
(3362) Khufu	0.99	0.47	0.70	271	0	-17.88	11.8	1e-02	–	–	–	2.9	0.16	1984 – 2005
(3551) Verenia	2.09	0.49	0.90	410	0	-14.12	9.9	3e-02	–	–	–	3.6	0.24	1983 – 2016
(3753) Cruithne	1.00	0.51	2.07	591	0	-8.06	4.2	2e-04	–	–	–	6.7	0.21	1973 – 2017
(3908) Nyx	1.93	0.46	1.00	1670	16	6.70	2.6	4e-07	7.20	1.6	1e-16	6.4	0.10	1980 – 2016
(4015) Wilson-H. ^C	2.64	0.63	4.00	897	0	-7.45	3.1	2e-04	–	–	–	10.7	0.50	1949 – 2016
(4034) Vishnu	1.06	0.44	0.42	488	1	-38.74	9.2	2e-16	-33.14	7.9	6e-16	4.9	0.20	1986 – 2015
(4179) Toutatis	2.54	0.63	5.40	5834	55	-14.50	3.7	1e-16	-2.67	0.5	1e-16	2.1	0.26	1933 – 2017
(4197) Morpheus [§]	2.30	0.77	1.80	694	6	30.64	11.3	8e-07	29.16	11.1	2e-06	2.9	0.60	1954 – 2016
(4581) Asclepius	1.02	0.36	*0.26	202	4	-30.78	16.8	4e-04	-19.69	5.6	4e-11	2.9	0.08	1988 – 2016
(4660) Nereus	1.49	0.36	0.33	527	32	5.25	5.4	7e-02	8.61	3.9	4e-05	6.1	0.04	1981 – 2015
(4688) 1980 WF	2.24	0.51	0.60	215	0	-7.00	5.5	5e-02	–	–	–	9.6	0.06	1980 – 2011
(4769) Castalia	1.06	0.48	1.40	298	15	-5.10	3.0	8e-03	-6.14	2.8	8e-04	10.5	0.12	1989 – 2016
(5011) Ptah	1.64	0.50	*1.86	582	0	-14.77	6.5	6e-05	–	–	–	6.2	0.45	1960 – 2016
(5693) 1993 EA	1.27	0.59	*1.62	1310	0	-8.67	4.5	4e-04	–	–	–	2.9	0.18	1983 – 2017
(6037) 1988 EG	1.27	0.50	*0.65	407	8	-6.97	5.0	4e-03	-9.07	4.5	1e-04	9.3	0.08	1987 – 2016
(6239) Minos	1.15	0.41	*0.71	892	3	6.79	3.7	3e-04	7.98	3.5	1e-05	7.0	0.09	1982 – 2016
(6489) Golevka	2.49	0.61	0.53	980	40	-13.45	12.1	6e-02	-5.17	0.7	1e-16	1.8	0.05	1991 – 2016
(6611) 1993 VW	1.70	0.48	*1.48	1076	0	-5.06	4.2	4e-02	–	–	–	4.1	0.10	1982 – 2016
(7336) Saunders	2.31	0.48	*0.62	592	0	11.68	8.1	7e-03	–	–	–	3.5	0.16	1982 – 2011
(7341) 1991 VK	1.84	0.51	*1.62	1403	13	-4.41	3.5	7e-03	-2.44	0.8	3e-11	3.6	0.07	1981 – 2017
(7350) 1993 VA ^C	1.36	0.39	2.36	1185	0	-5.27	2.7	2e-04	–	–	–	4.6	0.21	1963 – 2016
(7822) 1991 CS	1.12	0.16	1.60	1151	4	8.03	5.6	4e-03	6.57	5.5	2e-02	3.7	0.20	1990 – 2016
(10302) 1989 ML	1.27	0.14	*0.49	418	0	29.66	5.1	1e-16	–	–	–	6.7	0.20	1989 – 2016
(10563) Izhdubar	1.01	0.27	*1.55	541	0	18.94	7.9	1e-04	–	–	–	3.4	0.46	1991 – 2016
(11054) 1991 FA ^C	1.98	0.45	*1.41	1183	0	-1.23	1.1	1e-02	–	–	–	16.6	0.03	1937 – 2016
(11405) 1999 CV3 [§]	1.46	0.39	*3.24	2130	0	9.79	5.8	7e-04	–	–	–	2.7	0.61	1978 – 2016
(13651) 1997 BR	1.34	0.31	0.56	824	2	-12.18	9.9	3e-02	-17.54	8.5	5e-04	2.4	0.19	1979 – 2017
(14402) 1991 DB	1.72	0.40	0.60	451	0	-8.57	5.5	2e-03	–	–	–	6.9	0.05	1990 – 2017
(29075) 1950 DA	1.70	0.51	2.00	521	12	-3.91	1.8	2e-05	-2.60	0.5	1e-16	13.7	0.09	1949 – 2016
(31221) 1998 BP26	1.72	0.26	*1.29	842	0	-17.85	6.1	7e-09	–	–	–	2.7	0.48	1997 – 2016
(33342) 1998 WT24	0.72	0.42	*0.93	1722	17	-10.46	9.2	1e-02	-16.32	2.5	1e-16	2.1	0.18	1998 – 2016
(37638) 1993 VB [†]	1.91	0.52	*0.49	99	0	38.32	32.9	5e-02	–	–	–	2.3	0.32	1993 – 2015
(37655) Illapa	1.48	0.75	*0.93	422	2	-11.72	3.6	4e-12	-10.86	3.4	7e-12	10.0	0.09	1994 – 2015
(41429) 2000 GE2	1.59	0.56	0.20	332	0	-31.28	14.9	1e-03	–	–	–	2.5	0.09	1997 – 2017
(53550) 2000 BF19	1.50	0.42	*0.56	212	0	-40.20	27.3	4e-02	–	–	–	2.5	0.39	1991 – 2016
(54509) YORP [†]	1.00	0.23	*0.10	548	5	-19.17	47.6	3e-01	-33.69	13.3	3e-09	0.7	0.06	2000 – 2005
(55408) 2001 TC2	1.10	0.22	0.46	136	0	-13.87	10.6	3e-02	–	–	–	6.7	0.11	1979 – 2017
(65679) 1989 UQ	0.92	0.26	0.92	411	0	-18.51	5.8	5e-08	–	–	–	6.9	0.25	1954 – 2017
(65690) 1991 DG	1.43	0.36	*0.54	252	0	-32.34	13.2	5e-05	–	–	–	3.5	0.31	1990 – 2016
(65717) 1993 BX3	1.39	0.28	*0.25	100	0	28.55	21.3	1e-02	–	–	–	2.7	0.13	1992 – 2016
(65733) 1993 PC	1.15	0.47	*0.74	382	0	-18.75	9.9	2e-03	–	–	–	3.0	0.20	1992 – 2015
(66400) 1999 LT7	0.86	0.57	0.41	241	0	-40.12	8.2	1e-15	–	–	–	4.2	0.17	1987 – 2014
(67399) 2000 PJ6 ^C	1.30	0.35	*0.81	249	0	-12.47	8.2	2e-02	–	–	–	7.4	0.17	1951 – 2016
(85770) 1998 UP1	1.00	0.35	*0.28	494	0	-17.35	5.7	2e-07	–	–	–	5.2	0.07	1990 – 2017
(85953) 1999 FK21	0.74	0.70	0.59	946	0	-10.34	2.5	1e-13	–	–	–	4.4	0.05	1970 – 2016

Table 1 continued

Table 1 (continued)

Name	a	e	D	N_o	N_r	$\langle da/dt \rangle$	σ	p	$\langle da/dt \rangle_r$	σ_r	p_r	s_Y	ξ	Arc
(85990) 1999 JV6	1.01	0.31	0.45	1032	15	-11.83	4.0	3e-07	-14.14	1.0	1e-16	3.9	0.07	1999 – 2017
(99907) 1989 VA	0.73	0.59	1.40	571	0	11.69	3.8	1e-07	–	–	–	7.4	0.17	1989 – 2016
(101955) Bennu [†]	1.13	0.20	0.49	569	29	-12.41	7.8	6e-05	-19.03	0.1	1e-16	4.9	0.16	1999 – 2013
(136582) 1992 BA	1.34	0.07	*0.36	167	0	-17.07	7.2	2e-04	–	–	–	4.5	0.12	1991 – 2017
(136770) 1996 PC1	1.84	0.45	*0.28	248	0	-7.98	5.1	1e-02	–	–	–	8.5	0.04	1996 – 2017
(136818) Selqet	0.94	0.35	*0.59	483	0	7.90	3.3	3e-05	–	–	–	8.8	0.07	1997 – 2016
(136993) 1998 ST49	2.31	0.59	*1.02	437	7	24.86	15.0	9e-04	29.07	14.9	1e-04	2.2	0.50	1998 – 2013
(137924) 2000 BD19	0.88	0.89	0.97	530	5	-22.53	13.7	1e-03	-25.86	10.5	1e-06	1.8	0.08	1996 – 2017
(138175) 2000 EE104	1.00	0.29	*0.31	844	3	-31.66	7.6	1e-12	-32.33	7.6	3e-13	2.6	0.16	1998 – 2017
(138852) 2000 WN10	1.00	0.30	*0.32	853	0	16.46	4.2	2e-13	–	–	–	4.8	0.08	2000 – 2017
(138911) 2001 AE2	1.35	0.08	*0.51	491	0	-14.36	9.4	7e-03	–	–	–	4.0	0.15	1984 – 2015
(152563) 1992 BF	0.91	0.27	0.27	330	0	-13.08	1.3	1e-16	–	–	–	14.0	0.04	1952 – 2017
(152671) 1998 HL3	1.13	0.37	0.30	305	0	-35.10	9.6	4e-12	–	–	–	3.8	0.16	1998 – 2017
(152754) 1999 GS6	1.19	0.50	0.41	275	0	-20.88	16.3	6e-03	–	–	–	2.2	0.12	1999 – 2016
(153201) 2000 WO107	0.91	0.78	0.51	423	0	-22.36	13.2	3e-03	–	–	–	2.1	0.05	2000 – 2017
(154590) 2003 MA3 [†]	1.11	0.40	*0.16	87	0	-38.28	19.2	3e-04	–	–	–	3.4	0.09	1997 – 2012
(162004) 1991 VE	0.89	0.66	*0.81	794	2	18.83	3.5	1e-16	21.84	2.8	1e-16	4.9	0.16	1954 – 2015
(162080) 1998 DG16	0.90	0.36	0.78	136	0	-18.25	7.1	1e-05	–	–	–	3.1	0.20	1980 – 2015
(162082) 1998 HL1	1.25	0.19	*0.59	267	0	-43.06	17.9	4e-05	–	–	–	2.1	0.46	1998 – 2016
(162117) 1998 SD15	0.93	0.34	*0.54	496	0	-9.07	1.7	1e-16	–	–	–	14.7	0.07	1998 – 2017
(162142) 1998 VR	0.88	0.32	*0.62	415	0	9.07	3.0	4e-07	–	–	–	9.8	0.09	1998 – 2017
(162162) 1999 DB7	1.21	0.19	*0.37	224	0	20.23	12.3	6e-03	–	–	–	3.7	0.13	1998 – 2016
(162173) Ryugu	1.19	0.19	*0.49	729	0	-15.99	6.7	2e-07	–	–	–	3.6	0.08	1986 – 2016
(162181) 1999 LF6	1.41	0.28	0.73	1297	2	-11.86	3.3	1e-12	-9.77	3.1	1e-09	5.0	0.13	1979 – 2017
(162361) 2000 AF6	0.88	0.41	*0.32	303	0	20.04	8.8	3e-05	–	–	–	4.0	0.09	1990 – 2014
(162463) 2000 JH5 [§]	1.15	0.24	1.05	484	0	-32.47	12.9	7e-07	–	–	–	2.2	0.58	2000 – 2016
(162783) 2000 YJ11	1.31	0.23	*0.25	125	0	-49.32	16.3	2e-08	–	–	–	3.5	0.22	2000 – 2015
(162911) 2001 LL5	1.20	0.34	*0.51	233	0	19.39	13.0	8e-03	–	–	–	3.1	0.16	2001 – 2017
(163023) 2001 XU1	0.80	0.55	*0.49	316	0	34.39	9.0	1e-16	–	–	–	2.9	0.18	2001 – 2017
(164202) 2004 EW [†]	0.99	0.28	*0.25	426	0	27.84	13.6	6e-04	–	–	–	2.4	0.11	2003 – 2015
(164206) 2004 FN18 ^C	1.70	0.41	*1.07	489	0	-4.96	4.0	2e-02	–	–	–	9.1	0.10	1954 – 2017
(164207) 2004 GU9	1.00	0.14	0.16	192	0	-32.12	11.8	6e-06	–	–	–	2.3	0.09	2001 – 2017
(174050) 2002 CC19 [§]	1.28	0.11	*1.12	363	0	60.23	20.5	3e-06	–	–	–	2.3	1.29	1985 – 2015
(188174) 2002 JC	0.82	0.39	*1.18	286	3	-19.53	12.2	2e-03	-12.08	10.5	3e-02	3.0	0.19	1991 – 2017
(190758) 2001 QH96 [§]	1.75	0.36	*0.78	196	0	49.52	27.3	1e-04	–	–	–	3.0	0.75	1994 – 2017
(192563) 1998 WZ6	1.45	0.41	*1.23	670	0	-19.56	7.9	1e-05	–	–	–	2.5	0.32	1998 – 2015
(203471) 2002 AU4	0.86	0.37	*0.47	356	0	-13.71	7.5	9e-04	–	–	–	6.5	0.09	1993 – 2017
(208023) 1999 AQ10	0.93	0.24	*0.30	329	3	-24.89	7.1	6e-14	-23.77	6.0	1e-16	4.7	0.12	1998 – 2017
(215442) 2002 MQ3 [†]	0.91	0.27	1.07	328	0	-20.40	12.0	4e-04	–	–	–	2.2	0.33	2002 – 2016
(216523) 2001 HY7	0.91	0.41	*0.27	288	0	30.74	6.0	1e-16	–	–	–	6.1	0.11	2001 – 2016
(230111) 2001 BE10	0.82	0.37	*0.54	746	3	-15.38	6.2	1e-07	-13.98	5.9	6e-07	4.7	0.10	2000 – 2016
(234341) 2001 FZ57	0.94	0.60	0.34	205	0	-26.41	20.2	5e-02	–	–	–	3.3	0.10	1991 – 2013
(235756) 2004 VC [§]	1.13	0.26	1.14	201	1	-32.67	15.6	2e-04	-32.36	15.6	2e-04	2.7	0.62	1992 – 2016
(249886) 2001 RY11 [§]	1.48	0.28	1.20	337	0	35.16	22.9	6e-03	–	–	–	2.4	0.80	1992 – 2015
(252399) 2001 TX44 [†]	0.87	0.55	0.29	132	0	-57.07	26.2	2e-03	–	–	–	2.2	0.19	2001 – 2014
(252558) 2001 WT1	1.09	0.40	0.53	206	0	-58.28	15.7	2e-07	–	–	–	2.8	0.46	2001 – 2017
(256004) 2006 UP [†]	1.59	0.30	*0.09	167	0	-65.21	19.5	2e-08	–	–	–	2.4	0.11	2002 – 2017
(267759) 2003 MC7 ^C	1.37	0.18	*0.62	300	0	-10.83	3.5	2e-08	–	–	–	14.4	0.13	1953 – 2017
(283457) 2001 MQ3 ^C	2.23	0.46	*0.54	310	0	-13.72	4.9	2e-07	–	–	–	14.1	0.15	1951 – 2012
(297418) 2000 SP43	0.81	0.47	0.41	672	1	-16.34	7.9	8e-07	-16.36	7.9	7e-07	2.9	0.08	2000 – 2017

Table 1 continued

Table 1 (continued)

Name	a	e	D	N_o	N_r	$\langle da/dt \rangle$	σ	p	$\langle da/dt \rangle_r$	σ_r	p_r	s_Y	ξ	Arc
(306383) 1993 VD	0.88	0.55	*0.18	101	0	-11.41	6.6	5e-03	—	—	—	7.1	0.02	1993 – 2017
(307070) 2002 AV31	1.31	0.25	*0.26	233	0	-22.98	11.5	2e-03	—	—	—	3.4	0.11	2001 – 2017
(310442) 2000 CH59	0.86	0.42	*0.37	340	0	28.82	6.8	3e-13	—	—	—	4.5	0.14	1999 – 2017
(326354) 2000 SJ344 [†]	1.14	0.17	*0.11	37	0	-43.98	42.9	5e-04	—	—	—	2.3	0.08	2000 – 2012
(326683) 2002 WP [†]	1.45	0.22	0.52	767	0	11.80	5.5	9e-06	—	—	—	4.6	0.12	2002 – 2017
(330659) 2008 GG2 [†]	1.59	0.28	*0.09	169	0	23.85	11.2	4e-04	—	—	—	4.7	0.04	2003 – 2016
(344074) 1997 UH9	0.83	0.47	*0.65	325	0	31.18	10.8	8e-07	—	—	—	3.0	0.27	1997 – 2017
(348306) 2005 AY28 [†]	0.87	0.57	*0.19	221	2	-76.16	23.2	1e-07	-79.90	23.1	4e-08	2.4	0.16	2004 – 2017
(350462) 1998 KG3	1.16	0.12	*0.14	170	0	-26.27	7.8	4e-10	—	—	—	5.2	0.06	1998 – 2013
(350523) 2000 EA14 [†]	1.12	0.20	*0.21	145	0	43.85	20.4	9e-04	—	—	—	2.4	0.16	1999 – 2013
(358453) 2007 EH88	1.12	0.44	*0.39	117	0	-41.28	25.2	2e-02	—	—	—	2.2	0.23	1993 – 2014
(363505) 2003 UC20 ^C	0.78	0.34	1.90	400	5	-4.24	0.9	1e-16	-4.41	0.9	1e-16	31.6	0.11	1954 – 2017
(363599) 2004 FG11 [†]	1.59	0.72	0.15	246	8	-33.78	7.9	2e-13	-37.35	7.2	1e-16	5.0	0.06	2003 – 2016
(364136) 2006 CJ [†]	0.68	0.75	*0.32	241	11	-25.18	11.2	1e-04	-38.38	1.8	1e-16	1.5	0.07	2005 – 2017
(373393) 1972 RB ^{†C}	2.15	0.49	*0.54	65	0	5.56	5.5	4e-02	—	—	—	22.5	0.06	1950 – 2016
(385186) 1994 AW1	1.11	0.08	*1.02	1589	3	4.10	2.8	3e-04	4.12	2.7	2e-04	6.3	0.08	1986 – 2017
(388189) 2006 DS14 [†]	0.86	0.34	0.32	197	0	-23.38	12.7	6e-03	—	—	—	3.5	0.10	2001 – 2014
(390522) 1996 GD1 [†]	1.19	0.35	*0.27	92	0	-29.07	16.9	7e-03	—	—	—	3.0	0.13	1996 – 2014
(399308) 1993 GD	1.10	0.24	*0.26	113	0	44.26	9.6	3e-12	—	—	—	5.7	0.19	1993 – 2015
(401885) 2001 RV17 [†]	0.91	0.34	*0.28	181	0	-19.09	8.8	4e-04	—	—	—	5.4	0.08	2001 – 2016
(412976) 1987 WC	1.36	0.23	*0.37	155	0	42.09	17.9	1e-04	—	—	—	3.2	0.29	1987 – 2015
(412977) 1990 UO	1.26	0.77	*0.45	115	0	44.74	25.7	7e-03	—	—	—	2.4	0.15	1990 – 2015
(415711) 1998 WT7 ⁸	1.15	0.11	*0.56	169	0	50.30	24.7	5e-04	—	—	—	2.1	0.51	1998 – 2015
(416151) 2002 RQ25 [†]	1.11	0.31	*0.26	230	6	16.71	12.9	5e-02	19.52	9.6	1e-03	3.4	0.08	2002 – 2017
(433953) 1997 XR2	1.08	0.20	*0.25	407	8	14.78	9.7	9e-03	11.65	7.7	9e-03	3.3	0.05	1997 – 2017
(437844) 1999 MN	0.67	0.67	*0.19	141	4	37.93	3.9	1e-16	37.42	3.8	1e-16	9.6	0.05	1999 – 2015
(441987) 2010 NY65 [†]	1.00	0.37	0.23	257	16	12.89	29.9	5e-01	-18.44	1.9	1e-16	1.0	0.06	2010 – 2017
(443837) 2000 TJ1	1.16	0.08	0.25	355	0	-9.71	7.1	2e-03	—	—	—	5.7	0.04	2000 – 2016
(452389) 2002 NW16	1.11	0.03	0.85	1107	0	-9.67	5.4	7e-04	—	—	—	2.9	0.15	2001 – 2017
(455146) 1993 FS	2.23	0.42	*0.43	103	0	38.44	17.9	7e-04	—	—	—	3.4	0.34	1992 – 2016
(455176) 1999 VF22	1.31	0.74	*0.27	134	0	-64.33	13.4	4e-12	—	—	—	4.4	0.15	1999 – 2016
(461353) 1999 LS7	1.01	0.30	*0.25	134	0	-48.53	22.9	4e-04	—	—	—	2.0	0.19	1999 – 2016
(467336) 2002 LT38 [†]	0.85	0.31	*0.28	307	0	11.67	6.2	2e-03	—	—	—	5.9	0.05	2002 – 2016
(468468) 2004 KH17 [†]	0.71	0.50	0.20	211	1	-43.87	5.4	1e-16	-43.86	5.4	1e-16	5.8	0.09	2004 – 2016
(469445) 2002 LT24 [†]	0.72	0.50	0.14	185	0	-26.83	19.7	4e-02	—	—	—	2.3	0.04	2002 – 2016
(470975) 2009 SC15 [†]	1.27	0.18	*0.19	241	2	-63.61	21.2	5e-07	-55.31	20.2	5e-06	2.1	0.19	2002 – 2016
(474158) 1999 FA	1.08	0.13	*0.26	225	0	-41.26	9.2	1e-16	—	—	—	2.2	0.20	1978 – 2017
(474163) 1999 SO5	1.09	0.07	*0.23	255	0	-28.61	11.5	2e-04	—	—	—	3.1	0.12	1999 – 2017
(480808) 1994 XL1	0.67	0.53	*0.23	186	0	-31.77	3.5	1e-16	—	—	—	16.0	0.07	1994 – 2017
(480883) 2001 YE4	0.68	0.54	*0.26	349	7	-47.11	2.1	1e-16	-50.06	0.6	1e-16	9.9	0.13	2001 – 2017
(481442) 2006 WO3	0.80	0.45	*0.17	291	0	-42.51	9.0	1e-16	—	—	—	3.7	0.09	2001 – 2017
(483656) 2005 ES70 [†]	0.76	0.39	*0.06	137	0	-72.82	5.1	1e-16	—	—	—	10.3	0.06	2004 – 2017
2004 SC56 [†]	0.77	0.43	0.29	180	0	-42.90	27.8	2e-03	—	—	—	1.7	0.15	2004 – 2010
2004 BG41 [†]	2.51	0.61	*0.05	90	0	-51.24	30.0	8e-03	—	—	—	1.9	0.04	2003 – 2016
2007 PB8 [†]	0.88	0.45	*0.23	80	0	-50.05	33.7	2e-02	—	—	—	1.5	0.15	2002 – 2012
2009 BD [†]	1.06	0.05	*0.01	190	0	-497.62	99.3	6e-13	—	—	—	0.6	0.07	2008 – 2011

8. COMPARISON WITH NUGENT ET AL. (2012)

8.1. Using matching observation intervals

We analyzed the 54 Yarkovsky objects described by Nugent et al. (2012) by constructing observation inter-

vals whose calendar years matched those listed in Table (3) of that work. We compared (Section 6) our results with their findings (Figure 1). We agreed with all $\langle da/dt \rangle$ values save one, (4179) Toutatis, for which we

found a z -score of 2.68. We examine this object in more detail in Section 13.5.

However, we also found that 23 objects that Nugent et al. (2012) identified as detections did not pass our detection threshold (Section 5.2). Much of this discrepancy is explained by this work’s higher threshold for detection — a p -value of 0.05 approximately corresponds to an S/N of 2, while Nugent et al. (2012) considered possible detections for objects with S/N > 1. Indeed, all but five of the 23 objects exhibit $1 < \text{S/N} < 2$ in Nugent et al. (2012)’s table.

8.2. Using all available data

When using all available data (including data that were not available for use by Nugent et al. (2012)), we found good agreement (Figure 2), except for two objects — (4179) Toutatis and (1620) Geographos — for which our drift rates do not match those of Nugent et al. (2012).

9. COMPARISON WITH FARNOCCHIA ET AL. (2013)

9.0.1. Using matching observation intervals

We analyzed the 47 Yarkovsky objects found by Farnocchia et al. (2013) using matching observation intervals (to the nearest calendar year) and compared (Section 6) our results with their findings. We found agreement on all $\langle da/dt \rangle$ values (Figure 3).

We found four objects — (105140) 2000 NL10, (326290) Akhenaten, (339714) 2005 ST1, and 2003 XV — that were considered to be detections by Farnocchia did not pass our detection thresholds (Section 5.2). However, all four of these discrepant objects are listed in Tables 3 and 4 of Farnocchia et al. (2013), indicating that they are either “less reliable” detections or have low S/N values.

9.1. Using all available data

When using all available data, we found relatively good agreement (Figure 4). However, we found three objects — (2100) Ra-Shalom, (326290) Akhenaten, and (6239) Minos — for which our drift rates do not match those of Farnocchia et al. (2013). We discuss these special cases in Section 13.6.

10. YARKOVSKY EFFICIENCY DISTRIBUTION

Equations 3 and 4 provide a mechanism to interpret the drift in semi-major axis $\langle da/dt \rangle$ in terms of physical parameters of the measured object. In particular, $\langle da/dt \rangle$ can be described in terms of the Yarkovsky efficiency, ξ , where $0 < \xi < 1$. However, the relationship between $\langle da/dt \rangle$ and ξ depends on density and diameter, and thus determination of ξ requires estimation of these physical parameters.

Diameters were extracted from the Small Body Database (SBDB) (JPL Solar System Dynamics 2017b, see also Section 12). Densities were assigned according to SMASS II taxonomic types, which we also extracted from the SBDB, using the mean densities reported by Carry (2012). Objects of unknown taxonomic type were assigned a density equal to the mean density (2470 kg/m^3) for the objects in our sample with known type.

We analyzed the distribution of ξ values and found a median Yarkovsky efficiency of $\xi = 0.12_{-0.06}^{+0.17}$ (Figure 5). Note that a bias in this estimate stems from our inability to report near-zero drift rates as Yarkovsky detections. Therefore, the true distribution of efficiencies is presumably shifted toward lower values than presented here.

Several objects exhibit Yarkovsky efficiencies that substantially exceed the median value of $\xi = 0.12$. For these objects, the non-gravitational influence, if real, may be unrelated to Yarkovsky (e.g., sublimation). It is also possible that some of the high-efficiency detections are fictitious (e.g., faulty astrometry). For these reasons, we added a cautionary flag to a dozen objects with Yarkovsky efficiencies above 0.5 in Table 1. We discuss two unphysical detections in Section 13.7.

11. SPIN ORIENTATION DISTRIBUTION

La Spina et al. (2004) provided an estimate of the ratio of retrograde to prograde rotators ($N_R/N_P = 2_{-0.7}^{+1}$) in the NEA population from a survey of spin vectors.

Measurements of the Yarkovsky drift rate can also be used to infer N_R/N_P , because objects with a positive $\langle da/dt \rangle$ are almost certain to be prograde rotators, while objects with a negative $\langle da/dt \rangle$ are almost certain to be retrograde rotators.

However, given a population of objects with estimated $\langle da/dt \rangle$ values, the best estimate of N_R/N_P is *not* equal to the ratio R of the number of objects with negative $\langle da/dt \rangle$ to the number with positive $\langle da/dt \rangle$. A bias occurs because each estimated $\langle da/dt \rangle$ value has an associated uncertainty, and there is thus a non-zero probability that an object with a measured positive $\langle da/dt \rangle$ value in fact has a negative $\langle da/dt \rangle$ value (and vice versa). Because there are more retrograde rotators than prograde rotators, this process will bias observers towards measuring a lower observed ratio, R_O , than is actually present.

This point can be illustrated with a simple (albeit exaggerated), analytic example. Consider four objects: A , B , C , and D . Objects A , B , and C all have $\langle da/dt \rangle$ values of $-10 \pm 25 \times 10^{-4} \text{ au/My}$, while object D has a $\langle da/dt \rangle$ value of $+10 \pm 25 \times 10^{-4} \text{ au/My}$. In this example, the true ratio, R_T , of the number of objects with negative $\langle da/dt \rangle$ to the number of objects with posi-

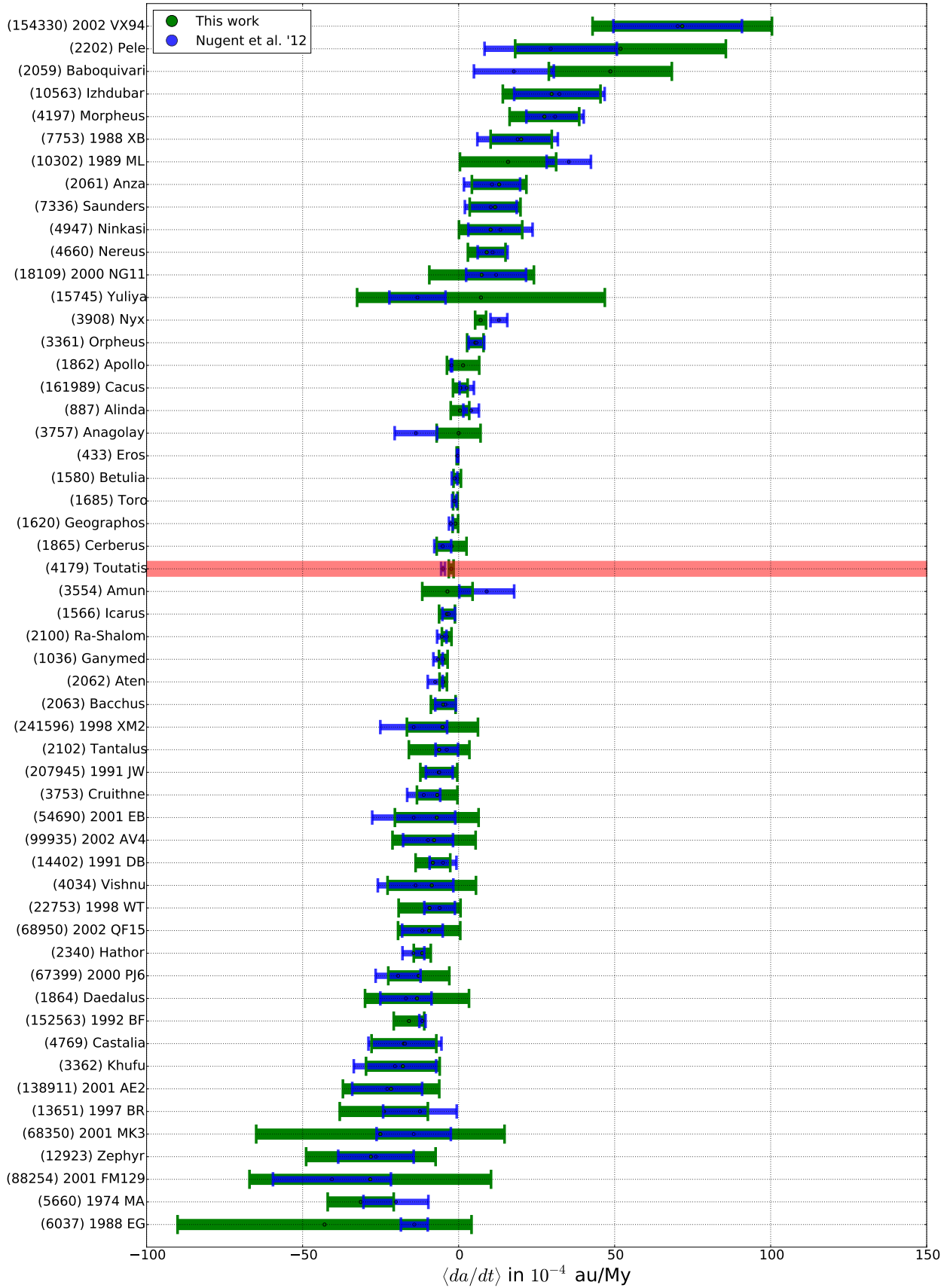


Figure 1. A comparison of our Yarkovsky detections (green) and those determined by Nugent et al. (2012) (blue), when we used only matching data. Measurements that disagreed (i.e., $z_i > 2$, Section 6) are highlighted in red. Objects are ranked from most positive to most negative Yarkovsky drift rate.

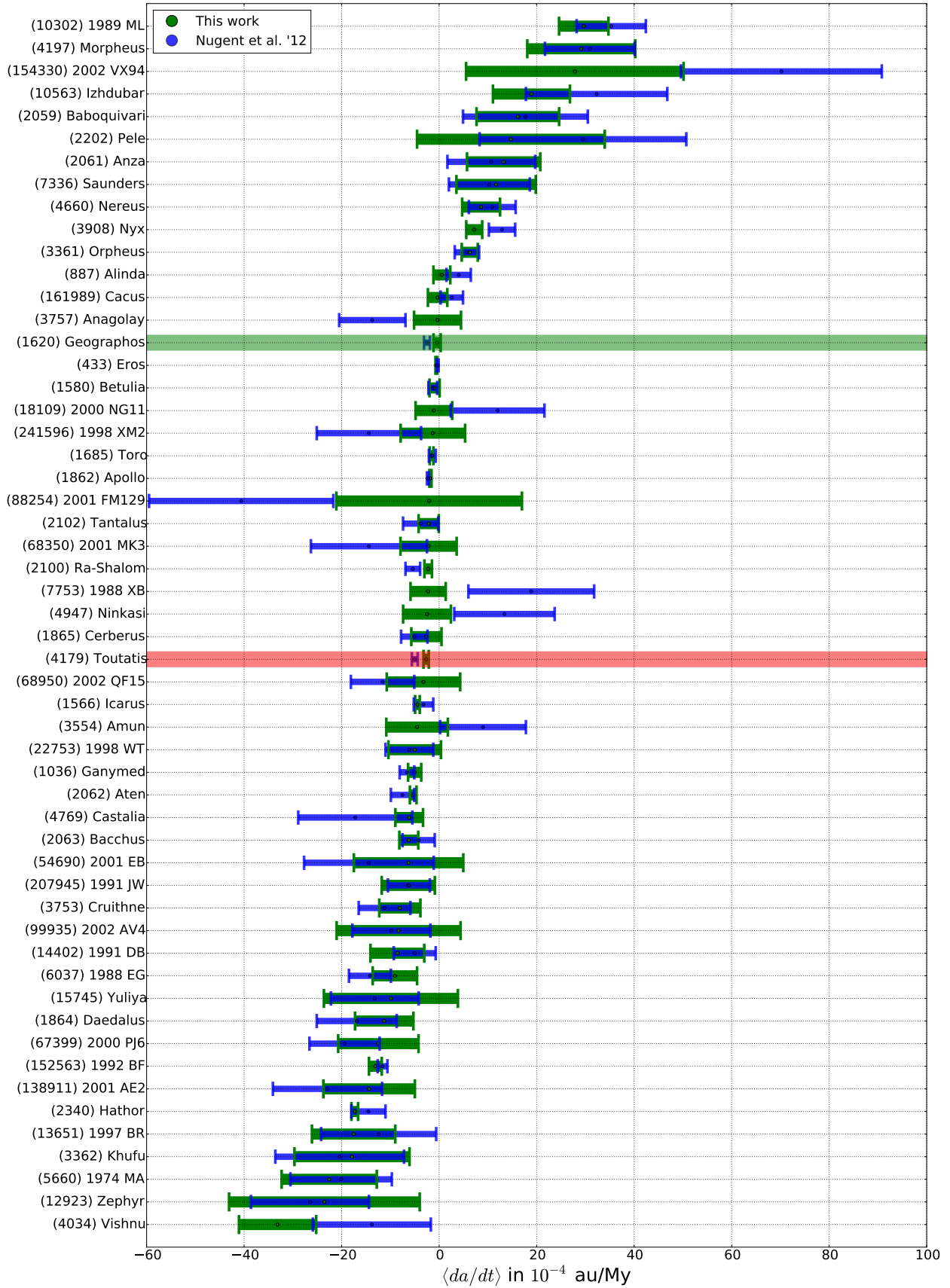


Figure 2. A comparison of our Yarkovsky detections (green) and those determined by Nugent et al. (2012) (blue), when we used all available data. Measurements that disagreed (i.e., $z_i > 2$, Section 6) only when using all available data are highlighted in green, while those that also disagreed when matching observational intervals are highlighted in red. Objects are ranked from most positive to most negative Yarkovsky drift rate.

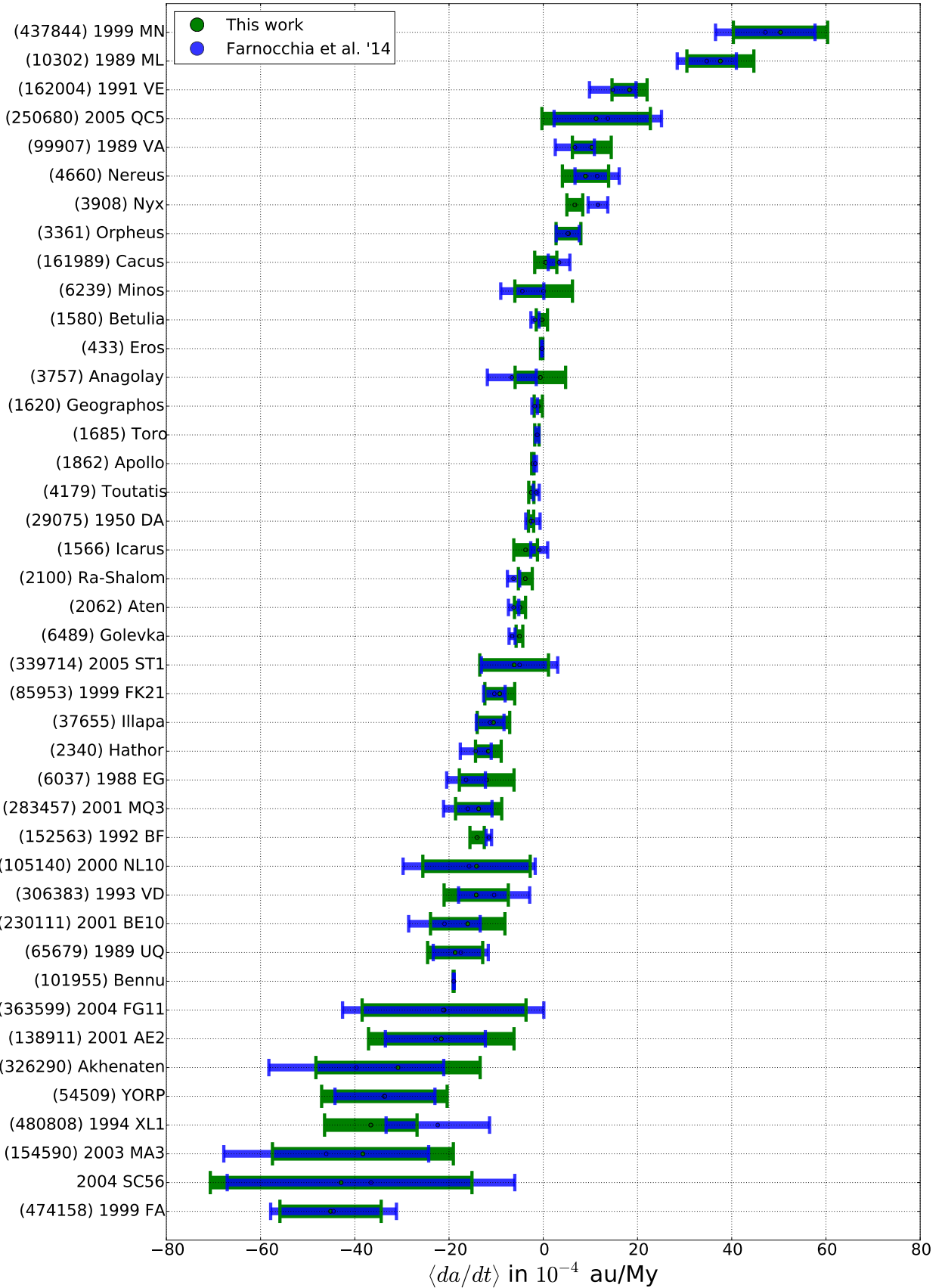


Figure 3. A comparison of our Yarkovsky detections (green) and those determined by Farnocchia et al. (2013) (blue), when we used matching data arcs. Measurements that disagreed (i.e., $z_i > 2$, Section 6) are highlighted in red. Some objects ((483656) 2005 ES70, 2003 XV, 2004 BG41, 2007 PB8, 2009 BD) were not included in this plot for display purposes, but all of them had $z_i \leq 2$. Objects are ranked from most positive to most negative Yarkovsky drift rate.

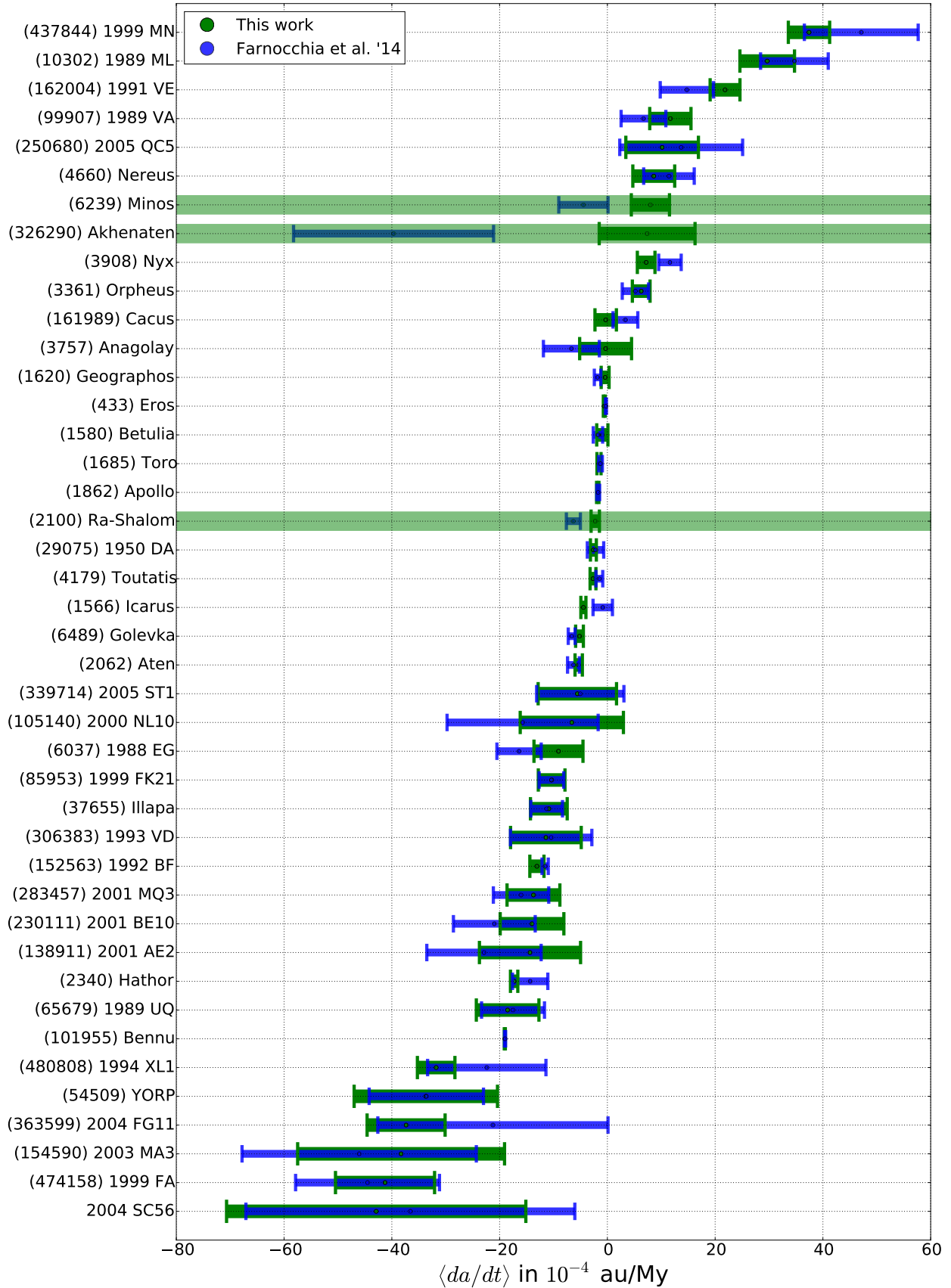


Figure 4. A comparison of our Yarkovsky detections (green) and those determined by Farnocchia et al. (2013) (blue), when we used all available data. Measurements that disagreed (i.e., $z_i > 2$, Section 6) are highlighted in green. Some objects ((483656) 2005 ES70, 2003 XV, 2004 BG41, 2007 PB8, 2009 BD) were not included in this plot for display purposes, but all of them had $z_i \leq 2$. Objects are ranked from most positive to most negative Yarkovsky drift rate.

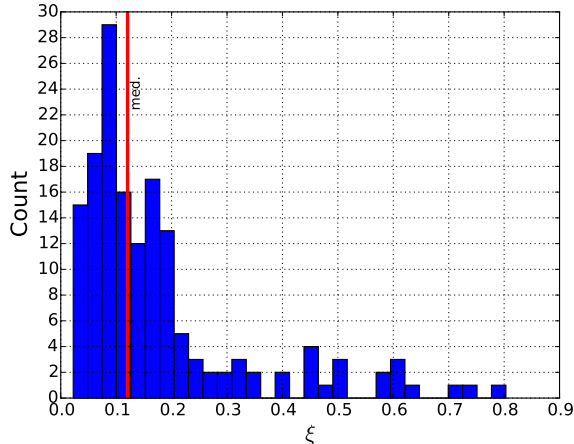


Figure 5. The distribution of Yarkovsky efficiencies ξ measured with our sample of 159 objects. Diameter and density assumptions are described in the text. The median efficiency, $\xi = 0.12$, is shown with a red vertical line. For clarity, we did not plot two objects with unphysical (>1) efficiencies (Section 13.7).

tive $\langle da/dt \rangle$ is $R_T = 3.0$. However, when an observer attempts to measure, for example, $\langle da/dt \rangle_A$, there is a $\sim 34\%$ chance that the observer will erroneously conclude that A has a positive $\langle da/dt \rangle$ value. In fact, we can calculate the probabilities associated with each of the five possible ratios that can be observed (Table 2) and demonstrate that one is most likely to observe $R_O = 1.0$. If 10,000 observers independently took measurements of objects A , B , C , and D , a plurality would conclude that $R_O = 1.00$, while a majority would agree that R_O lies between 0.0 and 1.0 — even though the true ratio is $R_T = 3.0$.

Table 2. The probability (P , rightmost column) of measuring a given ratio (R_O) of number of objects with $\langle da/dt \rangle < 0$ ($N_{<0}$) to number of objects with $\langle da/dt \rangle > 0$ ($N_{>0}$) for a sample of objects with true ratio $R_T = 3.0$ (Section 11). The true ratio is not the most likely result for an observer to measure.

$N_{<0}$	$N_{>0}$	R_O	P
4	0	∞	10%
3	1	3.00	34%
2	2	1.00	37%
1	3	0.33	17%
0	4	0.00	3%

Our data suggest that out of 159 objects, 114 have $\langle da/dt \rangle < 0$, for an observed ratio of $R_O = \frac{114}{159-114} = 2.53$. To approximate the true ratio R_T , we assumed

that the nominal ratio we measured was the most likely ratio for any observer to measure. Determining the true ratio is then a matter of simulating a universe with a set of simulated $\langle da/dt \rangle$ values that are consistent with our measured values, and also yield $R_O = 2.53$.

To find the value of R_T that corresponds to our measured R_O value, we ran a set of nested Monte Carlo simulations, using the following procedure:

1. Create a new ‘universe’, U_i .
 - (a) Within U_i , generate a set of 159 $\langle da/dt \rangle$ values, pulled from distributions consistent with our measurements. This set of $\langle da/dt \rangle$ values are the true values for the 159 objects in universe U_i . Therefore, R_T can be calculated (exactly) for this universe.
 - (b) Simulate what 10^4 independent observers in universe U_i would measure as an observed ratio, R_O .
 - (c) Determine the mean and standard deviation in observed ratio (R_O and σ_R , respectively) in universe U_i (Figure 6).
2. Repeat step 1 over many ($\sim 10^3$) universes, and record the set of resulting distinct R_T values, and corresponding R_O , σ_R values.
3. Determine the set of R_T values for which $R_O \pm \sigma_R$ encompasses our observed ratio of $R_O = 2.53$.

The resulting simulations suggest that the most likely true ratio for our observed 159 objects is $R_T = 2.9 \pm 0.4$.

If we wish to relate the ratio of retrograde-to-prograde rotators in our data to the corresponding ratio amongst the entire population of NEAs, we must also account for sampling errors, which will further broaden the uncertainties on R . The sampling uncertainty σ_S on a measured ratio of R from a sample of N objects can be calculated directly from the standard deviation of the binomial distribution, and is given by

$$\sigma_S \approx \sqrt{NR} \times \frac{R+1}{N-R}. \quad (11)$$

The sampling uncertainty for R is therefore $\sigma_S = 0.5$, which suggests a Yarkovsky-based estimate for the ratio of retrograde-to-prograde NEAs of

$$N_R/N_P = 2.9 \pm 0.7. \quad (12)$$

The ratio of retrograde-to-prograde rotators can in principle provide bounds on the fraction of NEAs that enter near-Earth space through the ν_6 resonance (Nugent et al. 2012; Farnocchia et al. 2013). The inference

is complicated by observational bias, namely an over-representation of Atens in the observed sample compared to their expected fraction in a debiased population. If we attempt to account for this bias in a manner similar to that described by Farnocchia et al. (2013), we find

$$N_R/N_{P(\text{debiased})} = 2.1 \pm 0.7, \quad (13)$$

which gives a probability of ν_6 provenance of $0.35^{+0.12}_{-0.18}$.

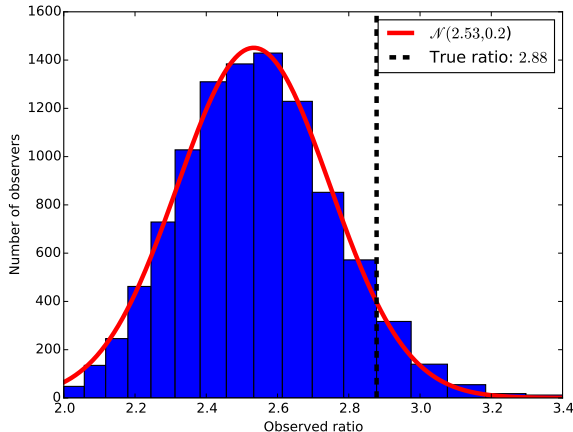


Figure 6. The number of observers measuring a given ratio R_O , for 10^4 independent observers measuring 159 simulated objects with $\langle da/dt \rangle$ values consistent with what we measured (Section 11). For a true ratio of $R_T = 2.9$, most observers will measure a ratio near $R_O = 2.53$. This bias must be corrected for when estimating the ratio of retrograde-to-prograde rotators from Yarkovsky observations.

12. YARKOVSKY EFFECT'S DIAMETER DEPENDENCE

Equations 3 and 4 illustrate the relationship between the magnitude of the Yarkovsky effect and the affected object's physical parameters. In particular, the theoretical formulation of this effect predicts a $D^{-1.0}$ dependence. Verifying this dependence with our data serves as a check on the theoretical underpinnings of the effect, and also validates our results.

We obtained diameter estimates for objects in our sample from JPL's SBDB (JPL Solar System Dynamics 2017b). For those objects with no listed diameter, we estimated the diameter from the object's H-magnitude using

$$D = \frac{10^{-0.2H}}{\sqrt{p_V}} 1329 \text{ km}, \quad (14)$$

with an assumed geometric albedo, p_V , of 0.14 (Stuart & Binzel 2004). If the uncertainty in diameter was

available in the SBDB, we used it, otherwise we set the uncertainty to a third of the diameter.

Here we note that while the analytical formulation of our Yarkovsky force model includes parameters that are dependent on the physical properties of the affected object (Section 4), the actual fit itself is dependent *only* on dynamics. In other words, our fits measure only the overall magnitude of the Yarkovsky acceleration, and are entirely agnostic about physical parameters such as diameter. Therefore, we can examine the Yarkovsky drift's dependence on diameter independently from the determination of the magnitude of the drift itself, and be confident that we are not committing a *petitio principii*.

We fit a power-law of the form

$$\langle da/dt \rangle = C \times D^p, \quad (15)$$

to describe the relationship between the magnitude of the Yarkovsky effect and the object diameter. We used an Orthogonal Distance Regression (ODR) (Jones et al. 2001–) algorithm to perform this fit, due to the potential errors present in both the dependent ($\langle da/dt \rangle$) and independent (D) variables (Figure 7). The resulting fit gave a best-fit power-law slope of $p = -1.05 \pm 0.06$. We verified the robustness of this result against the choice of diameter uncertainties, with values ranging from a fourth to two thirds of the diameter, and found consistent results. We also verified this result against different starting conditions on p . We discuss this result further in Section 14.4.

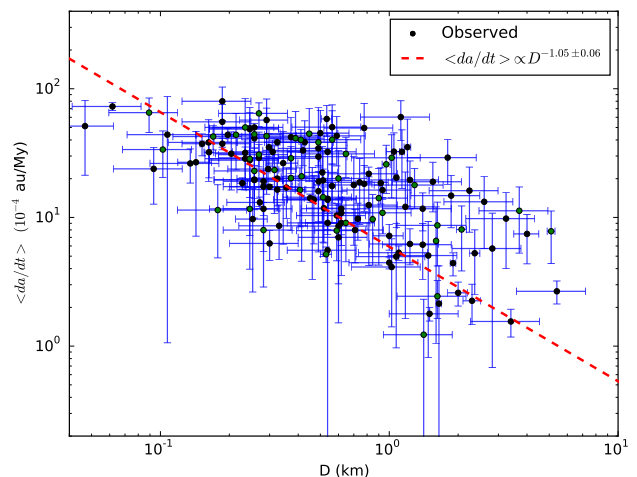


Figure 7. Drift rate $\langle da/dt \rangle$ as a function of object diameter, D . Diameters were either estimated from an H-magnitude (black) or extracted from the SBDB (green). Our analysis yields a diameter dependence of $D^{-1.05 \pm 0.06}$, consistent with the theoretical expectation for the Yarkovsky effect of $D^{-1.0}$.

13. OBJECTS OF INTEREST

13.1. (152563) 1992 BF

The 1992 BF astrometry includes four optical measurements taken in 1953. Vokrouhlický et al. (2008) showed that these points suffered from systematic errors due to faulty catalog debiasing, and re-analyzed these measurements to determine more accurate values. We used these corrected data, and determined $\langle da/dt \rangle = (-13.1 \pm 1.3) \times 10^{-4}$ au/My, which has a z-score of 1.62 with respect to Vokrouhlický et al. (2008)'s determination. The 1992 BF Yarkovsky drift was also measured with these points from 1953 discarded, which yielded $\langle da/dt \rangle = (-14.0 \pm 2.4) \times 10^{-4}$ au/My.

13.2. 2009 BD

Farnocchia et al. (2013) found a drift rate for 2009 BD of $\langle da/dt \rangle = (-493.4 \pm 58.8) \times 10^{-4}$ au/My. Following the work of Micheli et al. (2012), Farnocchia et al. (2013) also fit for a Solar Radiation Pressure (SRP) model for this object – which introduces a radial acceleration as a function of Area-to-Mass Ratio (AMR) – and found $\text{AMR} = (2.72 \pm 0.39) \times 10^{-4}$ m²/kg. Micheli et al. (2012) found $\text{AMR} = (2.97 \pm 0.33) \times 10^{-4}$ m²/kg with a solution that did not include Yarkovsky.

We also included an SRP component in our force model for 2009 BD, and found an area-to-mass ratio of $(2.21 \pm 0.40) \times 10^{-4}$ m²/kg, with a Yarkovsky drift rate of $\langle da/dt \rangle = (-497.6 \pm 40.5) \times 10^{-4}$ au/My. The drastic improvement in goodness-of-fit when both Yarkovsky and SRP models are included (Table 3) strongly supports the presence of these forces. We note that while our uncertainties on the drift rate appear to be around 20% better than those of Farnocchia et al. (2013), this may be due to the method by which we fit for $\langle da/dt \rangle$, which was performed as a secondary minimization after fitting for the dynamical state vector. Therefore, our uncertainties in $\langle da/dt \rangle$ do not account for correlation between parameters, and may be an underestimate because two related, non-gravitational effects are present.

13.3. (483656) 2005 ES70

The drift in semi-major axis for 2005 ES70 is $\langle da/dt \rangle = (-72.8 \pm 5.1) \times 10^{-4}$ au/My. Not only is this a strong effect, but it is also an unusually strong detection, with a *p*-value less than 10^{-16} , and an S/N greater than 14. Farnocchia et al. (2013) found $\langle da/dt \rangle = (-55.6 \pm 16.7) \times 10^{-4}$ au/My using pre-2013 astrometry, which is consistent with our re-analysis of this object using the same arc ($\langle da/dt \rangle = (-54.1 \pm 17.7) \times 10^{-4}$ au/My).

The drop in uncertainty by over a factor of three in four years is likely due to the increase in data coverage.

Table 3. Goodness-of-fit (χ^2) for 2009 BD, using various non-gravitational dynamical models, with 190 total observations prior to outlier rejection. The inclusion of both Yarkovsky forces and Solar Radiation Pressure (SRP) yields both a significantly lower χ^2 , as well as a decrease in the number of outliers, N_{out} .

<i>Model</i>	χ^2	N_{out}
Gravity-only	109	7
Yarkovsky	95	7
SRP	90	7
Yarkovsky+SRP	75	4

This object has a total of 132 optical and no radar observations since its discovery in 2005. Of these points, 48 were measured after 2011, and were therefore not included in the analysis performed by Farnocchia et al. (2013). This means that the dataset has increased in size by over 50% since 2011, and the arc has grown by 100%, which likely explains the drop in uncertainty.

The strength of this effect appears to be anomalous – however, when we account for this object's small size, we find that its drift rate is reasonable. Specifically, the diameter of 2005 ES70 is ~ 60 m, as calculated from an H-magnitude 23.8 (Equation 14), which corresponds to a Yarkovsky efficiency of $\xi = 0.06$, assuming a density of 2470 kg/m³.

13.4. (480883) 2001 YE4, (364136) 2006 CJ & (437844) 1999 MN

2001 YE4 has among the largest drift rates in this dataset, while also having amongst the smallest uncertainties, with $\langle da/dt \rangle = (-50.1 \pm 0.6) \times 10^{-4}$ au/My. The small uncertainty is largely explained by the seven radar measurements over three ranging apparitions — an analysis of the drift that does not include these points yields $\langle da/dt \rangle = (-47.1 \pm 2.1) \times 10^{-4}$ au/My, which means that the radar astrometry reduced the uncertainty by 70%. The drift rate, while large, corresponds to a Yarkovsky efficiency of $\xi = 0.13$, which is close to the median efficiency for the objects we analyzed.

Like 2001 YE4, 2006 CJ represents a strong Yarkovsky detection with $\langle da/dt \rangle = (-38.4 \pm 1.8) \times 10^{-4}$ au/My, and similarly, the relatively small uncertainty on this rate is largely due to radar observations. Our analysis includes 11 range and Doppler measurements of 2006 CJ from 2012 to 2017, and these points reduced the uncertainty on this detection by $\sim 85\%$.

With a drift rate of $\langle da/dt \rangle = (37.4 \pm 3.8) \times 10^{-4}$ au/My, 1999 MN is notable not only for the high drift rate and S/N, but also for having a semi-major axis that is increasing rather than decreasing. This ob-

ject’s small semi-major axis ($a = 0.67$ au), combined with a large eccentricity ($e = 0.67$), means that this object has a drift that is over twice as large as that of an asteroid at 1 au with low eccentricity with the same size and density. The Yarkovsky efficiency for 1999 MN is $\xi = 0.05$.

All three objects are part of an observational program designed to test general relativity and measure the oblateness of the Sun (Margot & Giorgini 2010; Verma et al. 2017). Their Yarkovsky drift rates will be taken into account in future analyses.

13.5. (4179) *Toutatis*

(4179) *Toutatis* is the only object in our sample for which our rate disagreed with a previous work’s result when using similar observation intervals – namely, our rate of $\langle da/dt \rangle = (-2.4 \pm 0.8) \times 10^{-4}$ au/My has a z -score of 2.7 when compared to Nugent et al. (2012)’s rate of $\langle da/dt \rangle = (-5.0 \pm 0.6) \times 10^{-4}$ au/My. Our rate when using all available data, $\langle da/dt \rangle = (-2.7 \pm 0.5) \times 10^{-4}$ au/My, is also not consistent with the previous work’s result.

Our rates do agree with Farnocchia et al. (2013), who found $\langle da/dt \rangle = (-1.5 \pm 0.6) \times 10^{-4}$ au/My. Farnocchia et al. (2013) suggest that this object’s passage through the Main Belt may make its orbit particularly sensitive to the number and mass of gravitational perturbers.

Another curiosity surrounding *Toutatis* is the drastic change in drift rate that we found when including radar observations, compared to using only optical observations – including radar observations results in an apparent $\sim 80\%$ drop in the calculated drift rate.

We found that the difference $\langle da/dt \rangle_o - \langle da/dt \rangle_{r+o}$ between *Toutatis*’s optical-only drift rate and the radar+optical drift rate is a strong function of the mass of the 24 Main Belt perturbing objects included in our force model. The perturbers included in our integration account for only $\sim 50\%$ of the total mass of the Main Belt. Artificially increasing the overall mass of these perturbers brings the $\langle da/dt \rangle_o$ value into closer agreement with the $\langle da/dt \rangle_{r+o}$ value. An incomplete dynamical model may therefore explain the discrepancy between *Toutatis*’s optical-only rate and radar+optical rate.

A final peculiarity about *Toutatis* is that its orbit can be determined without any optical astrometry. We fit our gravity-only and Yarkovsky models to the 55 radar measurements obtained over 5 apparitions. The solutions are almost exactly the same as the solutions that include optical astrometry (Table 4). Furthermore, a trajectory fit using only radar data is consistent with optical data – the radar-only trajectory yields a goodness-

of-fit of $\chi_{\text{opt}}^2 = 1775$ with 11,580 degrees-of-freedom, when compared with optical data.

These results suggest that the 55 radar observations over 5 apparitions are enough data to obtain a trajectory that is better than one inferred from over 11,000 distinct optical measurements.

Table 4. *Toutatis*’s orbital elements at epoch 01-JAN-2000 00:00:00 UTC, as determined from radar+optical data, and differences in orbital element values obtained between the optical-only and radar+optical Yarkovsky solutions ($\Delta_{\text{o-only}}$), and between the radar-only and radar+optical Yarkovsky solutions ($\Delta_{\text{r-only}}$). The tiny deviations in the last column suggest that optical astrometry is not necessary to determine *Toutatis*’s orbit. Orbital elements include i , inclination with respect to J2000.0 ecliptic frame, Ω , longitude of the ascending node, ω , argument of pericenter, and M , mean anomaly at epoch.

Orb. element	radar+optical	$\Delta_{\text{o-only}}$	$\Delta_{\text{r-only}}$
a (au)	2.51055095174	1.6e-09	1.7e-10
e	0.63428478950	2.8e-10	6.6e-10
i (deg)	0.46970438367	6.6e-07	5.4e-08
Ω (deg)	128.36720962273	4.2e-05	2.2e-05
ω (deg)	274.68317363284	3.7e-05	2.2e-05
M (deg)	-76.29635453165	8.7e-07	6.4e-08

13.6. (2100) *Ra-Shalom*, (326290) *Akhenaten*, and (6239) *Minos*

These objects are those for which we found statistically different results for the drift rate when comparing between our analysis with modern data, and the analysis performed by Farnocchia et al. (2013) using pre-2013 data. Our drift rates do match Farnocchia et al. (2013)’s rates when using the same observational intervals (Section 9).

We find a drift rate of *Ra-Shalom* $\langle da/dt \rangle = (-2.25 \pm 0.77) \times 10^{-4}$ au/My, while Farnocchia et al. (2013) found $\langle da/dt \rangle = (-6.31 \pm 1.3) \times 10^{-4}$ au/My using pre-2013 data. 264 new optical observations have been added since 2013, resulting in a $\sim 20\%$ increase in the size of the data set. While this is not a very large increase, the observations since 2013 also include the longest continuous set of observations ever taken for *Ra-Shalom*, of around five months, or $\sim 1/2$ of an orbit (here we define a set of observations as continuous if there is no period spanning more than two weeks without at least one measurement within the set). Characterization of the Yarkovsky effect is aided by greater orbital coverage – therefore, we expect this modern set of observations

to provide better constraints for this object than was previously possible.

For Akhenaten, we found a drift rate of $\langle da/dt \rangle = (7.38 \pm 8.9) \times 10^{-4}$ au/My, while Farnocchia et al. (2013) found $\langle da/dt \rangle = (-39.7 \pm 18.6) \times 10^{-4}$ au/My using pre-2013 data. Not only do these rates differ drastically in both magnitude and direction, but we also do not consider Akhenaten a Yarkovsky detection ($p = 0.11$). There have been fewer than 20 new observations of this object since 2012 (a $\sim 7\%$ increase).

A clue for the sudden change in apparent drift rate for Akhenaten can be found by examining the goodness-of-fit metric using pre-2013 data, χ_{old}^2 , and comparing with the metric when using all data, χ_{new}^2 . In particular, after outlier rejection, the pre-2013 fit had $\chi_{\text{old}}^2 = 171$ for 273 data points, while the fit using all data had $\chi_{\text{new}}^2 = 151$ for 287 data points. In other words, with the additional data, χ^2 dropped significantly. This is a strong indicator that the difference in results between the two fits may be due to outlier rejection – namely, that a small number of points were found to be faulty measurements with the addition of new data. If this were the case, one would expect these points to fall near the outlier rejection threshold when fitting using pre-2013 data. We expect that these faulty observations may have been responsible for producing a false Yarkovsky detection.

We indeed found three observations of Akhenaten, taken on the same night from the same observatory (644 Palomar), that were rejected from the modern analysis, but avoided rejection in the analysis using pre-2013 data. The three points had residuals of 2.1σ , 1.9σ , and 2.7σ , respectively. Other than 8 observations from the prior night, they were the only measurements of Akhenaten over a ten year period. Removing these three points from the pre-2013 data and re-fitting resulted in a new goodness-of-fit of $\chi_{\text{old}}^2 = 135$ (a $\sim 10\%$ decrease), and resulted in a Yarkovsky drift rate of $\langle da/dt \rangle = (0.91 \pm 18.28) \times 10^{-4}$ au/My, which is consistent with a non-detection. Temporally isolated observations can have a disproportionate effect on a calculated drift rate. When these observations are also few in number, they render the perceived rate particularly susceptible to faulty astrometry.

Finally, for Minos we find a rate of $\langle da/dt \rangle = (7.98 \pm 3.54) \times 10^{-4}$ au/My, while Farnocchia found $\langle da/dt \rangle = (-4.45 \pm 4.57) \times 10^{-4}$ au/My using pre-2013 data. The number of observations for this object has increased by over 50% since 2011, while the length of the observation interval has increased by 25%. The much larger data set explains our low p -value ($p = 10^{-5}$), and the shift in the measured effect.

13.7. (174050) 2002 CC19 and (1036) Ganymed

(174050) 2002 CC19 and (1036) Ganymed are the only two objects in our data set with unphysical ($\xi > 1$) Yarkovsky efficiency, with efficiencies of $\xi = 1.29$ and $\xi = 4.12$, respectively.

2002 CC19's high efficiency may be due to an incorrect diameter or density assessment – this object's spectral type is not known, so it was assigned a density of 2470 kg/m³ (Section 10). If this object had a lower density, perhaps closer to that typical of C-types, it would drive the ξ value to realistic levels.

Ganymed, however, is a different story. This object's high Yarkovsky efficiency is far too high to be explained by an uncertain density. However, the data for Ganymed stand out for several reasons. This object has measurements starting in 1924, and thus has one of the longest observational arcs we considered. It also has one of the largest sets of observations ($N = 5252$). Nugent et al. (2012) found $\langle da/dt \rangle = (-6.6 \pm 1.5) \times 10^{-4}$ au/My, consistent with ours ($\langle da/dt \rangle = (-5.0 \pm 1.3) \times 10^{-4}$ au/My), and devoted a section in their article to this anomalous case. Farnocchia et al. (2013) determined a drift rate ($\langle da/dt \rangle = (-6.1 \pm 1.6) \times 10^{-4}$ au/My) consistent with Nugent et al. (2012)'s and ours, but marked it as a potentially spurious detection, due to the unexpected strength of the drift rate relative to asteroid Bennu's rate scaled for diameter. Both Nugent et al. (2012) and Farnocchia et al. (2013) suggested that this detection may be due to older, potentially faulty measurements introducing a false signal. Nugent et al. (2012) also explored the impact of an incorrect size or mass determination.

To examine the possibility that some of the Ganymed astrometry is faulty, we re-ran our Yarkovsky determination process after discarding observations prior to successively later starting dates (Figure 8). We found that the detected drift rate abruptly disappears if data prior to 1951 are discarded. This fact, combined with the unphysically large Yarkovsky efficiency required for Ganymed to have a drift rate $|\langle da/dt \rangle| > 1.5 \times 10^{-4}$ au/My, leads us to believe that this object represents either a false Yarkovsky detection, or a drift rate that has been artificially magnified by poor, early astrometry.

13.8. Binary asteroids

Our sample of objects include four confirmed binary asteroids – (1862) Apollo, (136993) 1998 ST49, (363599) 2004 FG11, and (385186) 1994 AW1. Binaries present an opportunity to infer thermal properties from a Yarkovsky measurement, because tight constraints can

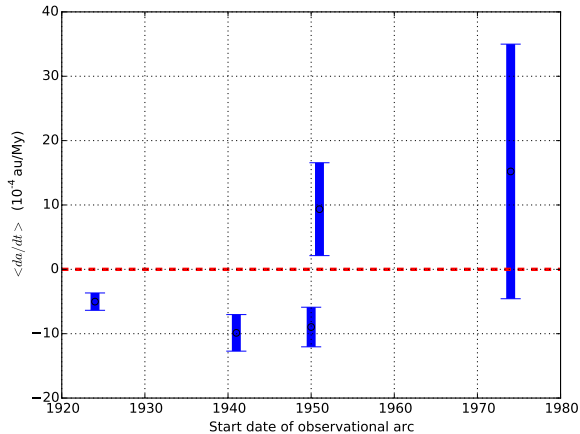


Figure 8. With a drift rate of $\langle da/dt \rangle = (-5.0 \pm 1.3) \times 10^{-4}$ au/My, (1036) Ganymed appears to have an unphysical Yarkovsky efficiency of $\xi = 4.12$. We find that if observations prior to 1950 are discarded, the Yarkovsky effect for this object appears to abruptly disappear. Ganymed may have an unreliably determined drift rate due to faulty older astrometry.

be placed on both mass and obliquity for these objects (Section 14.3, Margot et al. 2015).

14. DISCUSSION

14.1. Population-based detection verification

We have presented a statistical test which can be used to verify that a Yarkovsky detection is valid. However, one might still make the argument that the detections presented herein are merely due to statistical fluctuations. After all, the Yarkovsky effect often results in extremely small variations in an orbit. Perhaps the detections we present are really just a side effect of adding an extra degree of freedom to the gravity-only dynamical model.

Given the number of objects in our samples, we can address these concerns by looking for verifications of our detections on a population level, in addition to object-by-object. One such verification is the correspondence between the measured $\langle da/dt \rangle$ -vs- D inverse relationship, and the relationship predicted by the Yarkovsky theory (Section 12). It seems unlikely that a process which is merely fitting for statistical noise would generate the $1/D$ behavior that we expect *a priori*.

Another population-level analysis considers the distribution of spin poles of NEAs. We have already discussed how we measured the ratio of retrograde-to-prograde rotators in our sample (Section 11). We can also use the raw number of negative $\langle da/dt \rangle$ values compared to positive $\langle da/dt \rangle$ values to test the “statistical noise hypothesis”. Namely, we can ask the following question:

if our dynamical model, purportedly measuring a non-gravitational force, were instead merely overfitting for statistical noise, what would be the probability that we would have measured the number of retrograde rotators that we saw in our sample? In other words, what is the probability P of achieving a particular number m (or more) negatively-signed $\langle da/dt \rangle$ values in a population of N objects?

This question can be rephrased in terms of the probability P of observing at least m heads after N coin flips, for a coin weighted with probability p . This can be answered using the binomial distribution,

$$P = 1 - B(m - 1, N, p). \quad (16)$$

In our sample, we have $m = 114$ objects with a negative $\langle da/dt \rangle$ out of $N = 159$ objects total. To determine p , we first assume that the non-gravitational dynamical model *is* in fact overfitting for noise. In that case, the extraneous parameter would not favor one sign or another – in other words, the distribution of $\langle da/dt \rangle$ values that are measured should have a median of 0, which would suggest $p = 0.5$.

Putting these values into Equation 16, we find $P = 2.2 \times 10^{-8}$. In other words, if the model were merely measuring statistical noise, the odds of finding the ratio of negatively-signed to positively-signed drift rates observed in our data set (or a ratio more extreme) is approximately 1 in 46 million. This extremely low value provides an *ab absurdo* refutation of the hypothesis that we are fitting for noise. Note that this probability was calculated with minimal assumptions about the nature of the underlying statistical noise – we need only assume some distribution with a median of $\langle da/dt \rangle = 0$.

14.2. The viability of Yarkovsky measurements

For those objects with previous Yarkovsky detections, we have compared results from two previous works (namely, Nugent et al. (2012) and Farnocchia et al. (2013)) and found excellent agreement (Section 6). The general strength and consistency of the agreement when using roughly similar observation intervals (where we found disagreement on drift rates for only a single object) serves as a validation of the methods employed by all three groups. The agreement when we used all data available to us (where we found disagreement on drift rates for only five objects) speaks to the viability of measuring this small effect from astrometric measurements, because the measured rates are stable, even with the addition of new data.

Among this work and the two previous studies, at least three different orbital integration packages were used to perform the analyses, indicating robustness of the results against numerical implementations.

14.3. Interpreting ξ

We have found that within our sample of objects, typical Yarkovsky efficiencies lie between 0.06 – 0.29 (Section 10). An in-depth interpretation of these values would require a full thermal model of each object. However, we can still provide insights by making the simplifying assumption that all absorbed photons are re-emitted equatorially. Then the ξ values can be interpreted relative to the obliquity and thermal properties of the object in one of three ways:

1. If all the reradiated photons were emitted at the same phase lag of $\phi = \pm 90^\circ$, then the obliquity would be $\gamma \sim \arccos \xi$. With these assumptions, our typical ξ values suggest a range of obliquities $73^\circ < \gamma < 87^\circ$ or $93^\circ < \gamma < 107^\circ$.
2. If the obliquity, γ , were 0° or 180° , and all the reradiated photons were emitted at the same phase lag, then the phase lag would be $|\phi| \sim \arcsin \xi$. With these assumptions, typical efficiencies of $0.06 < \xi < 0.29$ imply phase lags of $3^\circ < |\phi| < 17^\circ$.
3. If the obliquity were $\gamma = 0^\circ$ or $\gamma = 180^\circ$, and the phase lag were $\phi = \pm 90^\circ$, then ξ could be interpreted as a measure of the distribution of photons that are emitted around ϕ .

Item (1) seems unlikely, given that we expect most of these objects to have obliquities near 0° or 180° – Hanuš et al. (2013) found that among a sample of 38 NEAs, more than 70% had $\gamma < 30^\circ$ or $\gamma > 150^\circ$. Item (2) is more palatable, and its applicability is protected by the cosine function’s slow dropoff, which means that assuming very high or very low spin pole latitudes will introduce errors of less than 10% for those objects with $\gamma < 30^\circ$ or $\gamma > 150^\circ$.

Rubincam (1995) derived an expression for phase lag as a function of thermal inertia Γ of a body rotating at frequency ν , and found

$$\phi = \arctan \left(\frac{\Gamma \sqrt{\nu}}{\Gamma \sqrt{\nu} + \sqrt{32\sigma T_0^3}} \right), \quad (17)$$

where σ is the Stefan-Boltzmann constant, and T_0 is the temperature of the body when it is at a distance a from the Sun.

With a typical thermal inertia of $\Gamma = 200 \text{ J m}^{-2} \text{ s}^{-\frac{1}{2}} \text{ K}^{-1}$ (Delbo et al. 2007), Equation 17 yields a phase lag of $\phi = 8.7^\circ$ for a body orbiting at a distance of 1 au and rotating with a period of 4.5 hours. Assuming $\gamma = 0^\circ$ or $\gamma = 180^\circ$, our median Yarkovsky efficiency of $\xi = 0.12$ suggests $|\phi| = 7^\circ$, which is in good agreement with the phase lag derived from thermal properties. With a more

complete thermal model, it should be possible to relate any of the differences between these two determinations to the distribution of re-emitted photons (Item (3) above).

Better knowledge of γ and ξ will yield tighter constraints on thermal properties of NEAs. In particular, the obliquity and mass of binaries can be accurately determined through dynamical measurements of the system. Therefore, binaries with Yarkovsky estimates (Section 13.8) will likely provide the best constraints on thermal properties in the future.

14.4. Expected diameter dependence

Delbo et al. (2007) suggested that, due to a dependence between thermal inertia, Γ , and diameter, one might expect a flatter $\langle da/dt \rangle$ diameter dependence than predicted by a theory that disregards correlation between these parameters. In particular, they found that

$$\Gamma \propto D^{-p}, \quad (18)$$

where $p \sim 0.4$.

Delbo et al. (2007), citing Vokrouhlický (1999), wrote

$$\langle da/dt \rangle \propto D^{-1} \frac{\Theta}{1 + \Theta + 0.5\Theta^2}, \quad (19)$$

where

$$\Theta = \frac{\Gamma}{\epsilon \sigma (\sqrt{2} T_0)^3} \sqrt{\frac{2\pi}{P}}, \quad (20)$$

where σ is the Stefan-Boltzmann constant, P is the rotation period, ϵ is the thermal emissivity, and T_0 is the temperature of the body when it is at a distance a from the Sun.

Delbo et al. (2007) suggested that because the asymptotic behavior (i.e., $\Theta \gg 1$) of Equation 19 gives

$$\langle da/dt \rangle \propto D^{-1} \Theta^{-1}, \quad (21)$$

then, by relating Equations 18, 20, and 21, one would find

$$\langle da/dt \rangle \propto D^{-1+p} \propto D^{-0.6}. \quad (22)$$

However, few objects yield values for Θ such that Equation 21’s pre-requisite of $\Theta \gg 1$ is appropriate. For example, typical objects in our sample have $P = 4.5$ hours and $T_0 = 300 \text{ K}$. With typical thermal inertias in the range $\Gamma \sim 200 - 400 \text{ J m}^{-2} \text{ s}^{-0.5} \text{ K}^{-1}$, Equation 20 yields $\Theta \sim 1 - 2$. In fact, because Equation 19 peaks at $\Theta = 1.4$, the slope of the function with respect to Θ near $\Theta = 1 - 2$ is nearly 0, which suggests $\langle da/dt \rangle \propto D^{-1} \Theta^0 \propto D^{-1}$.

We find $\langle da/dt \rangle \propto D^{-1.05 \pm 0.06}$ (Section 12), which is consistent with the nominal theory.

14.5. Drift determination and radar ranging

While the Yarkovsky effect can be measured for objects with no radar ranging data, range astrometry aids greatly in improving the accuracy of drift determination. In particular, the number of distinct radar apparitions with range data correlates strongly with reduced uncertainty in an object’s drift rate.

Of the 159 objects we analyzed, 53 had radar astrometry. Of these, 46 objects had range measurements. We examined the improvement in the Yarkovsky determination – quantified by σ_o/σ_{r+o} , or the ratio of the drift uncertainty without radar to that with radar – compared to the number of radar range apparitions for that object (Figure 9). We found that on average, each additional radar range apparition corresponds to an improvement in the precision by a factor of ~ 1.6 .

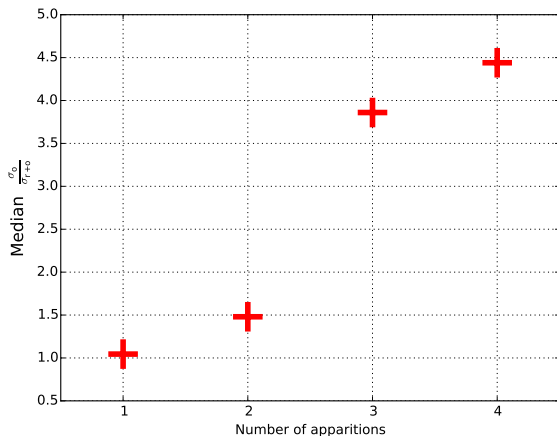


Figure 9. The ratio of the drift uncertainty without radar to that with radar, σ_o/σ_{r+o} , as a function of the number of radar apparitions during which ranging data were taken. The number of objects with radar range measurements were 24, 12, 7, and 3, for 1, 2, 3, and 4 apparitions, respectively.

15. CONCLUSION

With new astrometry and improved methods, we found a set of 159 NEAs with a measurable Yarkovsky drift. We found generally good agreement with previous studies. Most NEAs exhibit Yarkovsky efficiencies in a relatively small (0–0.2) range. We verified the Yarkovsky drift rate’s inverse dependence on asteroid size, and we estimated the ratio of retrograde-to-prograde rotators in the NEA population. In addition, we provided an estimate of the improvement in Yarkovsky determinations with the availability of radar data at multiple apparitions. Our results provide compelling evidence for the existence of a non-gravitational influence on NEA orbits.

16. ACKNOWLEDGEMENTS

We are grateful for the help and insights provided by Alec Stein regarding the statistical analyses of our data.

AHG and JLM were funded in part by NASA grant NNX14AM95G and NSF grant AST-1109772. Part of the work done here was conducted at Arecibo Observatory, which is operated by SRI International under a cooperative agreement with the National Science Foundation (AST-1100968) and in alliance with Ana G. Méndez-Universidad Metropolitana (UMET), and the Universities Space Research Association (USRA). The Arecibo Planetary Radar Program is supported by the National Aeronautics and Space Administration under Grant Nos. NNX12AF24G and NNX13AQ46G issued through the Near-Earth Object Observations program. This work was enabled in part by the Mission Operations and Navigation Toolkit Environment (MONTE). MONTE is developed at the Jet Propulsion Laboratory, which is operated by Caltech under contract with NASA. The material presented in this article represents work supported in part by NASA under the Science Mission Directorate Research and Analysis Programs.

REFERENCES

- Bottke, Jr., W. F., Vokrouhlický, D., Rubincam, D. P., & Nesvorný, D. 2006, *Annual Review of Earth and Planetary Sciences*, 34, 157
- Carry, B. 2012, *Planet. Space Sci.*, 73, 98
- Chesley, S. R., Baer, J., & Monet, D. G. 2010, *Icarus*, 210, 158
- Chesley, S. R., Vokrouhlický, D., Ostro, S. J., et al. 2008, in *Asteroids, Comets, Meteors 2008*, Vol. 1405, 8330
- Delbo, M., dell’Oro, A., Harris, A. W., Mottola, S., & Mueller, M. 2007, *Icarus*, 190, 236
- Evans, S., Taber, W., Drain, T., et al. 2016, in *The 6th International Conference on Astrodynamics Tools and Techniques (ICATT)*, International Conference on Astrodynamics Tools and Techniques, Darmstadt, Germany.
<https://indico.esa.int/indico/event/111/session/30/contribution/177/material/paper/0.pdf>
- Farnocchia, D., Chesley, S., Chamberlin, A., & Tholen, D. 2015, *Icarus*, 245, 94
- Farnocchia, D., Chesley, S. R., Chamberlin, A. B., & Tholen, D. J. 2015, *Icarus*, 245, 94
- Farnocchia, D., Chesley, S. R., Vokrouhlický, D., et al. 2013, *Icarus*, 224, 1
- Folkner, W. M., Williams, J. G., Boggs, D. H., Park, R. S., & Kuchynka, P. 2014, *Interplanetary Network Progress Report*, 196, 1
- Greenberg, A. H., Margot, J. L., Verma, A. K., et al. 2017, *AJ*, 153, 108
- Hanuš, J., Brož, M., Durech, J., et al. 2013, *AAp*, 559, A134
- Jones, E., Oliphant, T., Peterson, P., et al. 2001–, *SciPy: Open source scientific tools for Python*, .
<http://www.scipy.org/>
- JPL Solar System Dynamics. 2017a, JPL Radar Astrometry Database, <https://ssd.jpl.nasa.gov/?grp=ast&fmt=osod&radar=>, ,
- . 2017b, JPL Small Body Database, <https://ssd.jpl.nasa.gov/sbdb.cgi>, ,
- La Spina, A., Paolicchi, P., Kryszczyńska, A., & Pravec, P. 2004, *Nature*, 428, 400
- Mandel, J. 1964, *The Statistical Analysis of Experimental Data* (Dover Publications)
- Margot, J. L., & Giorgini, J. D. 2010, in *IAU Symposium*, Vol. 261, *IAU Symposium*, ed. S. A. Klioner, P. K. Seidelmann, & M. H. Soffel, 183–188
- Margot, J. L., Pravec, P., Taylor, P., Carry, B., & Jacobson, S. 2015, in *Asteroids IV*, ed. P. Michel, F. E. DeMeo, & W. F. Bottke (Univ. of Arizona Press), 355–373
- Micheli, M., Tholen, D. J., & Elliott, G. T. 2012, *NA*, 17, 446
- Minor Planet Center. 2017, Minor Planet database, http://minorplanetcenter.net/db_search, ,
- Nugent, C. R., Margot, J. L., Chesley, S. R., & Vokrouhlický, D. 2012, *Astronomical Journal*, 144, 60
- Rubincam, D. P. 1995, *JGR*, 100, 1585
- Stuart, J. S., & Binzel, R. P. 2004, *Icarus*, 170, 295
- Verma, A. K., Margot, J. L., & Greenberg, A. H. 2017, *Astrophys. J.*, in press
- Vokrouhlický, D. 1999, *A&A*, 344, 362
- Vokrouhlický, D., Chesley, S. R., & Matson, R. D. 2008, *AJ*, 135, 2336